Article

TRANSPARENT PROCESS OPEN ACCESS

EMBO reports

A secreted factor NimrodB4 promotes the elimination of apoptotic corpses by phagocytes in *Drosophila*

Bianca Petrignani[1,*], Samuel Rommelaere[1], Ketty Hakim-Mishnaevski[2], Florent Masson[1], Elodie Ramond[1], Reut Hilu-Dadia[2], Mickael Poidevin[3], Shu Kondo[4], Estee Kurant[2] & Bruno Lemaitre[1,**]

Abstract

Programmed cell death plays a fundamental role in development and tissue homeostasis. Professional and non-professional phagocytes achieve the proper recognition, uptake, and degradation of apoptotic cells, a process called efferocytosis. Failure in efferocytosis leads to autoimmune and neurodegenerative diseases. In *Drosophila*, two transmembrane proteins of the Nimrod family, Draper and SIMU, mediate the recognition and internalization of apoptotic corpses. Beyond this early step, little is known about how apoptotic cell degradation is regulated. Here, we study the function of a secreted member of the Nimrod family, NimB4, and reveal its crucial role in the clearance of apoptotic cells. We show that NimB4 is expressed by macrophages and glial cells, the two main types of phagocytes in *Drosophila*. Similar to *draper* mutants, *NimB4* mutants accumulate apoptotic corpses during embryogenesis and in the larval brain. Our study points to the role of NimB4 in phagosome maturation, more specifically in the fusion between the phagosome and lysosomes. We propose that similar to bridging molecules, NimB4 binds to apoptotic corpses to engage a phagosome maturation program dedicated to efferocytosis.

Keywords apoptotic cell; bridging molecule; *Drosophila*; Nimrod; phagocytosis
Subject Categories Autophagy & Cell Death; Development; Membranes & Trafficking
DOI 10.15252/embr.202052262 | Received 8 January 2021 | Revised 22 June 2021 | Accepted 30 June 2021
EMBO Reports (2021) e52262

Introduction

The clearance of apoptotic cells by phagocytes is an essential process during development and for the maintenance of tissue homeostasis (Arandjelovic & Ravichandran, 2015). Defective apoptotic cell clearance affects organ function and leads to the release of cytotoxic molecules and the development and progression of inflammatory and immune responses (Elliott & Ravichandran, 2010; Nagata *et al*, 2010; Poon *et al*, 2014). Recent studies also point to the importance of apoptotic cell clearance in the brain, as excessive or reduced phagocytosis can lead to neurodegeneration (Etchegaray *et al*, 2016; Purice *et al*, 2016; Hakim-Mishnaevski *et al*, 2019; Hilu-Dadia & Kurant, 2020). Efferocytosis, the phagocytosis of apoptotic cells, is a multi-step process often mediated by professional phagocytes such as macrophages and glia. It begins with the identification of the target cells by receptors that recognize specific "eat-me" signals that are exposed at the surface of apoptotic cells and distinguish them from living cells (Elliott & Ravichandran, 2016; Boada-Romero *et al*, 2020). One of the best characterized "eat-me" signals is phosphatidylserine (PS), a membrane phospholipid species usually found in the inner leaflet of the plasma membrane, but exposed on the surface of cells undergoing apoptosis (Segawa & Nagata, 2015; Nagata *et al*, 2016). Upon ligand recognition, phagocytic receptors engage downstream signaling pathways that initiate the uptake of the particle through an active and dynamic remodeling of the plasma membrane, which is mainly guided by the actin cytoskeleton (Pearson *et al*, 2003; Stuart & Ezekowitz, 2005; Melcarne *et al*, 2019a). Newly formed phagosomes undergo a maturation process to acquire digestive activity. The phagosome matures through fusion with endosomes and lysosomes, a process involving small GTPases of the Rab family (Kinchen & Ravichandran, 2010). Rab5 regulates the initial fusion events, by tethering early endosomes to the newly formed phagosome (Alvarez-Dominguez *et al*, 1996; Duclos *et al*, 2000; Kinchen *et al*, 2008). As the phagosome matures, Rab5 is replaced by Rab7 in a process called Rab conversion (Kinchen & Ravichandran, 2010; Poteryaev *et al*, 2010; Yousefian *et al*, 2013). Once recruited, Rab7 is responsible for inducing fusion of the phagosome and the lysosome, initiating acidification

1 Global Health Institute, School of Life Science, École Polytechnique Fédérale de Lausanne (EPFL), Lausanne, Switzerland
2 Department of Human Biology, Faculty of Natural Sciences, University of Haifa, Haifa, Israel
3 I2BC, CNRS, Université Paris-Saclay, Gif sur Yvette, France
4 Invertebrate Genetics Laboratory, Genetic Strains Research Center, National Institute of Genetics, Mishima, Japan
*Corresponding author. Tel: +41 21 693 06 28; E-mail: bianca.petrignani@epfl.ch
**Corresponding author (lead contact). Tel: +41 21 69 31831; E-mail: bruno.lemaitre@epfl.ch

and digestion of the corpse. A characteristic protein present on the phagolysosome membrane is lysosomal-associated membrane protein 1 (Lamp1), which is needed for lysosome fusion with the phagosome (Huynh *et al*, 2007). Less is known about the final stage of phagosome resolution and how the phagosome is resorbed to allow the phagocyte to return to homeostasis. However, studies have shown that bacteria-containing phagolysosomes in macrophages undergo fragmentation through vesicle budding and constriction (Levin *et al*, 2016; Botelho *et al*, 2020; preprint: Lancaster *et al*, 2020).

Recent studies in mammals have highlighted the importance of bridging molecules in the regulation of efferocytosis. Bridging molecules are secreted proteins that bind to the "eat-me" signal to provide a link between apoptotic cells and phagocytic receptors and enhancing recognition and phagocytosis of apoptotic cells (Savill & Fadok, 2000; Ravichandran, 2003, 2011). In mammals, several bridging molecules have been identified, including milk fat globule-epidermal growth factor 8 (MFG-E8) and growth arrest-specific 6 (Gas6) (Wu *et al*, 2006). Studies have shown that MFG-E8 binds in a Ca^{2+}-dependent manner to PS exposed at the surface of apoptotic cells, engaging their uptake by integrins αvβ3/5 (Hanayama *et al*, 2002; Borisenko *et al*, 2004; Kusunoki *et al*, 2012). Moreover, the absence of MFG-E8 in murine models causes a lupus-like autoimmune disease due to defective clearance of apoptotic cells (Huang *et al*, 2017). In *Caenorhabditis elegans* (*C. elegans*), the secreted protein TTR-52 mediates recognition of dying cells by linking PS with the phagocyte receptor CED-1 (Wang *et al*, 2010). While these studies have highlighted the relevance of bridging molecules in efferocytosis, the precise function of these molecules remains poorly understood. Some studies point to a role during the early phase of phagocytosis, facilitating apoptotic cell uptake, while others suggest that bridging molecules orient the maturation of the phagosome (Peng & Elkon, 2011; Galvan *et al*, 2012). The mechanism underlying efferocytosis has been well characterized in *Drosophila* (Serizier & McCall, 2017; Davidson & Wood, 2020). In this insect, three phagocytic receptors, the α-PS3/βν integrin heterodimer, Draper, and SIMU, have been identified for their role in the uptake of apoptotic cells (Freeman *et al*, 2003; Manaka *et al*, 2004a; Kurant *et al*, 2008; Nagaosa *et al*, 2011; Nonaka *et al*, 2013; Roddie *et al*, 2019). Studies have shown that the phagocytic ability of embryonic glia to engulf and degrade apoptotic neurons is determined by both SIMU and Draper. SIMU is required for recognition and engulfment of apoptotic neurons by glia, whereas Draper is mostly needed for their degradation (Kurant *et al*, 2008; Shklyar *et al*, 2014). Flies deficient for the two main receptors for apoptotic cells, Draper and SIMU, are viable but their lifespan is reduced and their central nervous system accumulates apoptotic bodies (Draper *et al*, 2014; Etchegaray *et al*, 2016). Although several engulfment receptors in *Drosophila* have been identified, little is known about their mechanism of action. So far, no bridging molecules have been identified in *Drosophila*.

In this study, we find that NimB4, a secreted protein of the Nimrod family, binds to apoptotic corpses in a PS-dependent manner to promote phagocytosis of apoptotic cells by glia and macrophages (also called plasmatocytes). Macrophages from *NimB4* mutants show defective phagocytosis of apoptotic cells *ex vivo*. Similar to *draper* mutants, *NimB4* mutants accumulate apoptotic cells in both embryonic and larval phagocytes, and exhibit motor defect in larvae and reduced lifespan of adults. Further functional studies reveal the role of NimB4 in phagosome maturation, notably in the formation of the phagolysosome. Collectively, this study identifies the first secreted factor involved in the phagocytosis of apoptotic cells in *Drosophila* and suggests an evolutionarily conserved role of bridging molecules in efferocytosis.

Results

NimB4 is a secreted protein enriched in phagocytes

To identify potential bridging molecules, we searched for secreted proteins expressed in phagocytes that could promote the phagocytosis of apoptotic cells. We focused our attention on secreted members of the Nimrod superfamily with characteristic EGF-like repeats (Bork *et al*, 1996; Callebaut *et al*, 2003; Kurucz *et al*, 2007), transmembrane Nimrod proteins have already been implicated in phagocytosis of bacteria (NimC1, Eater) or apoptotic corpses (SIMU, Draper), and in macrophages sessility and adhesion (Eater). In addition to these receptors, there are five secreted proteins of the Nimrod family called NimB1, B2, B3, B4, and B5 (Ju *et al*, 2006; Kurucz *et al*, 2007; Somogyi *et al*, 2008). Of these, only NimB5 has been characterized and has been shown to regulate peripheral hematopoiesis (Ramond *et al*, 2020). As bridging molecules are usually secreted by phagocytes, we monitored the expression of these five NimBs in macrophages of third-instar larvae. Consistent with a recent transcriptome analysis (Ramond *et al*, 2020), RT–qPCR analysis showed that NimB4 was the most highly expressed NimB member in macrophages (Fig 1A). To track the expression of NimB4 at the subcellular level, we generated a transgenic fly line carrying a V5-sGFP-tagged *NimB4* fusion under its own regulatory sequences, derived from the Dresden pFlyFos collection (Sarov *et al*, 2016). We used this reporter gene to follow NimB4 during embryonic and larval stages with a focus on glia and macrophages. At the embryonic stage, NimB4-sGFP appeared to be strongly enriched exclusively in macrophages (Fig 1B), whereas at the larval stage NimB4-sGFP was expressed in both macrophages and glial cells (Figs 1C and D, and EV1A). Live and fixed imaging of third-instar larval macrophages showed that NimB4-sGFP is present intracellularly. Live confocal imaging showed that NimB4-sGFP localizes in small dots throughout the cytoplasm, suggesting a localization in the endosomal compartment (Fig 1C).

To investigate whether expression of *NimB4* was modulated upon tissue damage, we collected larvae after clean injury with a thin needle in the anterior dorsal cuticle and monitored *NimB4* expression in the two major immune-responsive tissues, the fat body, and hemocytes. We observed that clean injury induces *NimB4* expression in hemocytes with an acute phase profile 1 h following challenge (Fig EV1B). In contrast, the transcription of *NimB4* in the fat body remained low and unchanged (Fig EV1C).

NimB4 binds to apoptotic cells

NimB4 is predicted to be a secreted protein due to the presence of a signal peptide (Somogyi *et al*, 2008). We generated a transgenic fly lines carrying a *UAS-NimB4-RFP* insertion and overexpressed *NimB4-RFP* in the fat body using the fat body-specific Gal4 driver

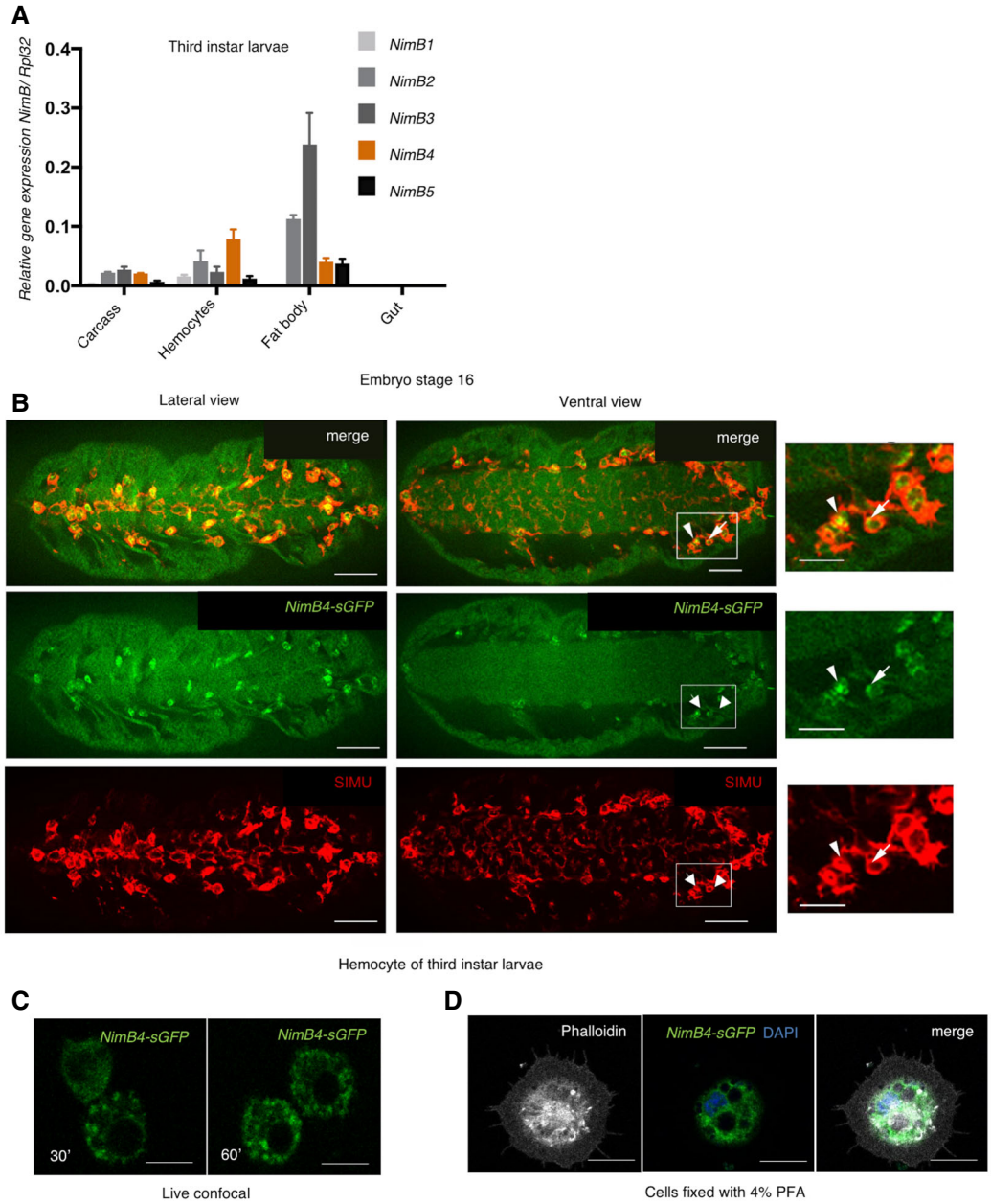

Figure 1. *NimB4* is enriched in phagocytes.

A RT–qPCR analysis of *NimB1, NimB2, NimB3, NimB4,* and *NimB5* transcripts, normalized to *RpL32*, from carcass, macrophages, fat body, and gut of wild-type (w^{1118}) L3 wandering larvae. Data are represented as mean ± SD from three independent experiments.

B Representative confocal imaging of *NimB4-sGFP* macrophages of embryo at stage 16; lateral (left) and ventral (right) views; tissues were stained with anti-GFP (green, corresponding to *NimB4-sGFP)* and anti-SIMU antibodies (red, corresponding to macrophages). The arrows show the presence of *NimB4-sGFP* inside the embryonic macrophages. Scale bars = 20 μm.

C Representative live confocal imaging of *NimB4-sGFP* macrophages of L3 wandering larvae at 30 and 60 min after dissection. Scale bars = 10 μm.

D Representative confocal imaging of *NimB4-sGFP* macrophages of L3 wandering larvae after fixation. Cells were stained with phalloidin (gray), DAPI (blue), and anti-GFP (green, corresponding to *NimB4-sGFP*). Scale bars = 10 μm.

Lpp. Western blot analysis of larval hemolymph extracts confirmed that NimB4-RFP protein was enriched in the hemolymph, as expected for a secreted protein (Fig EV1D). Furthermore, a strong NimB4-RFP signal was detected in the nephrocytes (a filtrating organ involved in the removal of hemolymph proteins) when NimB4-RFP was expressed either from the fat body or the hemocytes (Fig EV1E and F) (Ivy *et al*, 2015; Troha *et al*, 2019).

MFG-E8 binds PS exposed at the surface of apoptotic cells in a Ca^{2+}-dependent manner, engaging their uptake by the integrin $\alpha_v\beta_{3/5}$ phagocytic receptor (Borisenko *et al*, 2004). To explore if NimB4 could

similarly bind to apoptotic cells, we incubated hemolymph containing NimB4-RFP with healthy S2 cells, or with S2 cells undergoing apoptosis. We observed that NimB4-RFP protein colocalized exclusively with the apoptotic cells, stained with carboxyfluorescein succinimidyl ester (CFSE; Figs 2B and D, and EV2A). The binding of NimB4 to apoptotic cells was specific as no binding was observed when labeled apoptotic corpses were incubated with a control secreted protein composed of the RFP protein fused to the signal peptide of the Viking protein (SP^{vkg}-RFP) (Liu *et al*, 2017) (Fig 2A and D).

We then repeated the same experiment, but pre-treated apoptotic cells with Annexin V, a protein that coats apoptotic cells by binding to PS (Engeland *et al*, 1998; Janko *et al*, 2013). Pre-incubation of apoptotic corpses with Annexin V strongly reduced the binding of NimB4-RFP to the apoptotic cells, supporting the notion that NimB4 binds to apoptotic corpses in a PS-dependent manner (Fig 2C and D).

Next, we investigated if NimB4 can bind to apoptotic cells *in vivo*. For this, we induced apoptosis by expressing the apoptosis activator *reaper* in the imaginal wing disk using the driver *Apterous-Gal4*. After induction of apoptosis, we observed the binding of NimB4-sGFP to the region of the wing disk that expressed *Apterous-Gal4* (Fig EV2B). Additionally, we observed the binding of NimB4 to apoptotic cells released in the hemolymph after clean injury. No binding was observed between apoptotic corpses and the secreted protein SPvkg-RFP (Fig EV2C and D). Collectively, our studies revealed that NimB4 has key features of a bridging molecule in that it is secreted and binds to apoptotic corpses in a PS-dependent manner.

NimB4-deficient animals accumulate apoptotic corpses during development

To investigate the role of NimB4 *in vivo*, we generated a null mutation in the *NimB4* gene by CRISPR-Cas9, referred to as $NimB4^{sk2}$. The $NimB4^{sk2}$ mutant has a 14bp deletion in the second exon, inducing a stop codon at amino acid 113 (Fig EV3A–C). We isogenized the $NimB4^{sk2}$ mutation by backcrossing into the w^{1118} *DrosDel* background. $NimB4^{sk2}$ homozygous flies were viable and did not show any striking morphological defect. We investigated the role of NimB4 in developmentally regulated apoptosis in the embryo and the larval brain (Kurant, 2011; Zheng *et al*, 2017). Stage 16 embryos were co-stained with an anti-SIMU antibody that marks macrophages, and anti-Dcp-1 that marks apoptotic cells by staining activated Death caspase-1 (Dcp-1). Macrophages of $NimB4^{sk2}$ mutants were normally localized throughout the embryo (Fig 3A). Interestingly, we noted an increased level of Dcp-1-positive apoptotic cells in $NimB4^{sk2}$ embryos. Embryonic macrophages of $NimB4^{sk2}$ but not wild-type embryos appeared highly vacuolated and full of apoptotic corpses, a phenotype reminiscent of the $draper^{\Delta 5}$ mutant (Kurant *et al*, 2008) (Fig 3A and B). This finding suggests that $NimB4^{sk2}$ phagocytes can engulf apoptotic corpses but are deficient in their degradation. *H99* embryos do not show any developmentally induced apoptosis as they carry a small deficiency that removes the three pro-apoptotic genes *head involution defective (hid)*, *reaper*, and *grim* (Chen *et al*, 1996). We recombined the *H99* deficiency and $NimB4^{sk2}$ to confirm that the vacuolization of $NimB4^{sk2}$ embryonic macrophages is indeed caused by the accumulation of apoptotic corpses. Consistent with this notion, *NimB4*-deficient macrophages in the apoptosis-null *H99* mutant background did not show any vacuoles or Dcp-1 staining (Fig 3A). This demonstrates that the vacuolization of $NimB4^{sk2}$ embryonic macrophages is linked to the accumulation of apoptotic corpses inside the cell.

Moreover, we observed that the brain of $NimB4^{sk2}$ larvae also displayed a greater amount of apoptotic cells than wild-type larvae (Fig 3C and D). These data demonstrate that NimB4 is required for proper clearance of apoptotic cells during embryonic and larval brain development.

Defective clearance of apoptotic cells may lead to lethality and organ dysfunction (Henson & Hume, 2006). Similarly to $draper^{\Delta 5}$ mutant, $NimB4^{sk2}$ third-instar larvae displayed a crawling defect, with a drastic reduction of linear movement (Fuentes-Medel *et al*, 2009) (Fig EV3D). In contrast, no crawling defect was observed in $NimC1^{1}$ deficient larvae lacking a phagocytic receptor involved in bacterial uptake (Melcarne *et al*, 2019b), indicating that this phenotype is specific to $draper^{\Delta 5}$ and $NimB4^{sk2}$ mutants. At the adult stage, the $draper^{\Delta 5}$ flies have a shortened lifespan and an age-dependent locomotor defect (Draper *et al*, 2014).

A single-cell transcriptomic atlas of the aging *Drosophila* brain (Davie *et al*, 2018) revealed that *NimB4* is also expressed in the adult glial cells, suggesting its involvement in the phagocytosis. To evaluate the importance of *NimB4* during aging, we monitored two phenotypes usually associated with neurodegeneration in $NimB4^{sk2}$ adult flies and found that similar to the $draper^{\Delta 5}$ mutant, $NimB4^{sk2}$ flies displayed a climbing defect (suggesting declining motor activity), and reduced life span (Fig EV3E and F).

NimB4 enhances efferocytosis

Having shown that *NimB4* is required for the elimination of apoptotic cells, we then investigated at which step of the efferocytosis process NimB4 is required, using macrophages of third-instar larvae. Since NimB4 is secreted and binds to apoptotic corpses, we analyzed whether NimB4 contributes to the initial phase of uptake. To this end, we incubated macrophages and apoptotic cells on ice to inhibit the engulfment process, without altering binding to the phagocytic cell (Pearson *et al*, 2003). Macrophages of $NimB4^{sk2}$ larvae bound apoptotic corpses to the same extent as wild-type cells (Fig 4A and B). Conversely, the number of apoptotic corpses bound to the cell membrane of $draper^{\Delta 5}$ macrophages was reduced. Scanning electron microscopy experiments confirmed that apoptotic corpses bind to $NimB4^{sk2}$ but not $draper^{\Delta 5}$ macrophages (Fig 4C). This indicates that, unlike the Draper receptor, NimB4 is not involved in the initial phagocytic step of binding.

We then investigated whether NimB4 is required for the subsequent step of phagocytosis, that is the engulfment of bound apoptotic corpses. For this, we tested the ability of $NimB4^{sk2}$ larval macrophages to internalize fluorescently labeled apoptotic bodies using an *ex vivo* phagocytic assay. Macrophages from wild-type, $NimB4^{sk2}$, $draper^{\Delta 5}$, and the double mutant $NimC1^{1}$, $eater^{1}$ were incubated for 30 min, 1 h, or 2 h with Alexa555 fluorescent apoptotic bodies, and flow cytometry was used to measure their phagocytic index. We found that, at 30 min, only the double mutant $NimC1^{1}$, $eater^{1}$ exhibited a reduced phagocytosis. At 1 h, we observed reduced phagocytosis in both $NimC1^{1}$, $eater^{1}$, and $draper^{\Delta 5}$ mutants. Interestingly, the $NimB4^{sk2}$ mutant exhibited reduced phagocytosis of apoptotic corpses at a later time point (2 h)

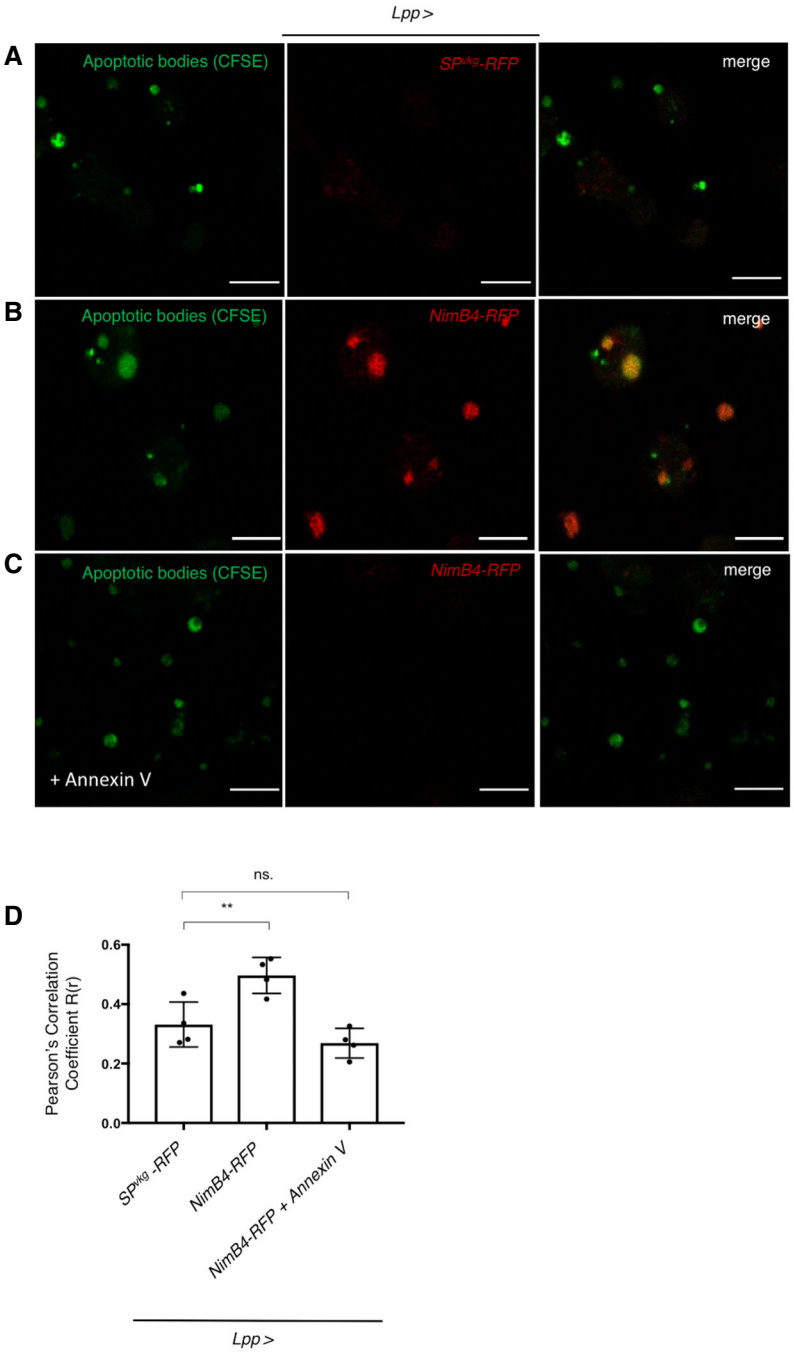

Figure 2. NimB4 binds to apoptotic cells *ex vivo*.

A–C Representative confocal imaging of CFSE-stained apoptotic bodies (green) incubated with secreted NimB4-RFP (B, C) or SP^{vkg}-RFP (A). Apoptotic bodies were pre-incubated in absence (A, B) or presence (C) of Annexin V (25 μg/ml). Scale bar = 10 μm.

D Quantification of the colocalization of NimB4-RFP or SP^{vkg}-RFP with the apoptotic bodies in presence or absence of Annexin V, as measured by Pearson's correlation coefficient. Values from at least four independent experiments are represented as mean ± SD (**$P < 0.01$ by ANOVA test followed by *post hoc* Dunnett's multiple comparison tests. ns: not significant).

compared to the wild type (Fig 4D). Use of a genomic fragment encompassing the *NimB4* gene rescued this decreased phagocytosis of the $NimB4^{sk2}$ mutant at 2 h (Fig 4D). Of note, $NimC1^{1}$; $eater^{1}$ mutants were unable to phagocytose apoptotic cells at all time points, indicating that the role of these two receptors is not restricted to bacterial phagocytosis.

To test if the role of NimB4 is specific to efferocytosis, we performed the same experiment with fluorescent AlexFluor488

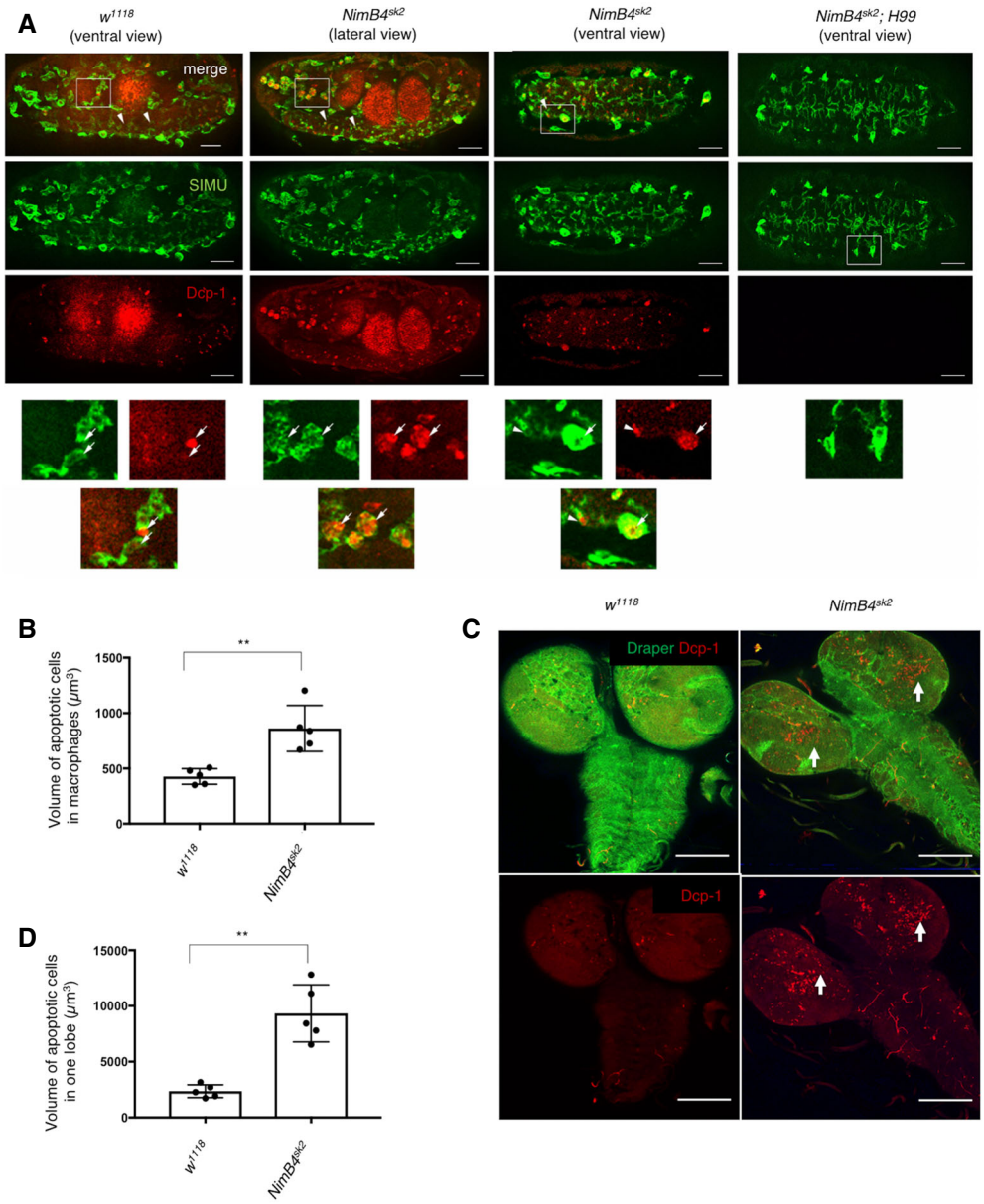

Figure 3. The *NimB4*^{sk2} mutant is defective in cell corpse clearance.

A Representative confocal imaging of wild-type (w^{1118}), *NimB4*^{sk2}, and apoptosis-null *NimB4*^{sk2}; *Df(3L) H99* embryonic macrophages at stage 16 of development; ventral and lateral view; Tissues were co-stained with Dcp-1 (red, corresponding to apoptotic corpses) and anti-SIMU (green, corresponding to macrophages) antibodies. The arrows show the presence of apoptotic cells inside embryonic macrophages. Scale bars = 20 µm.

B Quantification of caspase-positive particles (anti-Dcp-1, red) within macrophages (anti-SIMU, green). Values from at least five independent experiments are represented as mean ± SD total volume of caspase-positive particles (**$P < 0.01$, by Mann–Whitney test).

C Representative projections from confocal stacks of entire third-instar wild-type (w^{1118}) and *NimB4*^{sk2} larval brains stained with anti-Draper (green) and anti-Dcp-1 (red). The arrows show the presence of apoptotic cells in the central area of *NimB4*^{sk2} larval brain. Scale bars = 100 µm.

D Quantification of caspase-positive particles in the central brain area of larval brain. Values from at least five independent experiments are represented as mean ± SD total volume of caspase-positive particles (**$P < 0.01$, by Mann–Whitney test).

Staphylococcus aureus Bioparticles. Interestingly, *NimB4*^{sk2} macrophages retained the ability to phagocytose *S. aureus* bacteria at 2 h similar to the wild-type macrophages (Fig 4E). We included macrophages from *NimC1*^{1} *and eater*^{1} larvae that show impaired phagocytosis of bacteria as a positive control (Melcarne *et al*, 2019b). We conclude that NimB4 is not specifically required for the binding of apoptotic corpses but enhances phagocytosis of apoptotic cells.

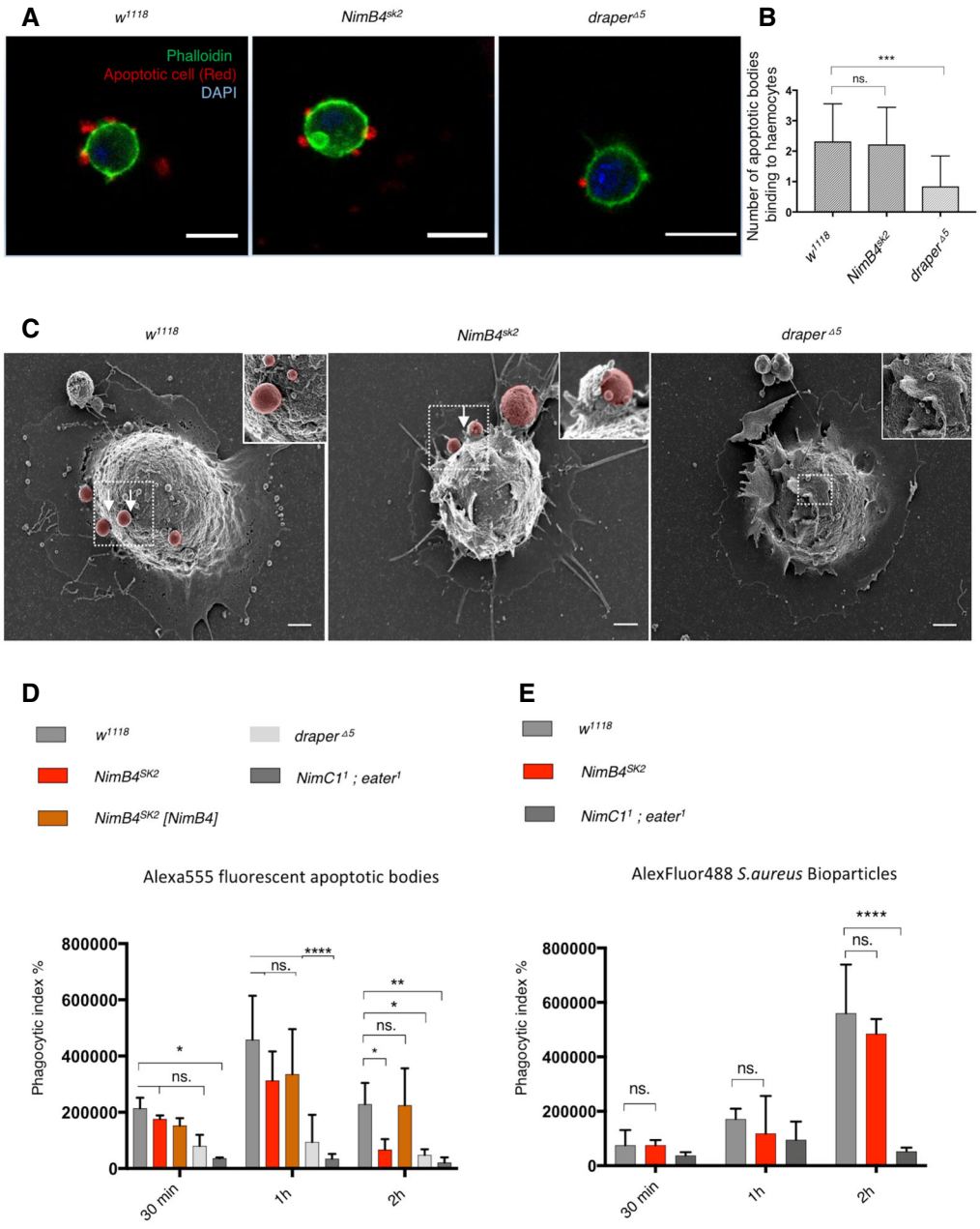

Figure 4. Phagocytosis of apoptotic cells is reduced in *NimB4^{sk2}* mutant.

A Representative confocal imaging of wild-type (*w^{1118}*), *NimB4^{sk2}*, and *draper$^{\Delta 5}$* macrophages incubated with fluorescently labeled apoptotic cells (red, CellTrace™ Red) on ice for 1 h and stained with Alexa Fluor™ 488 phalloidin (green). Scale bar: 10 μm.

B Quantification of the number of apoptotic cells (red) binding to the macrophages (green). Values from three independent experiments are represented as mean ± SD (***$P < 0.001$ by ANOVA test followed by *post hoc* Dunnett's multiple comparison tests. ns: not significant).

C Representative Scanning Electron Microscopy images of spread macrophages extracted from wild-type (*w^{1118}*), *NimB4^{sk2}*, and *draper$^{\Delta 5}$* L3 wandering larvae and incubated 30 min with apoptotic cells (artificially colored in red) at room temperature. The arrows show the binding of apoptotic cells to the macrophages. Scale bar: 1 μm.

D *Ex vivo* phagocytosis assay using Alexa555 fluorescent apoptotic bodies. Wild-type, *NimB4^{sk2}*, *NimB4* genomic rescue (*NimB4^{sk2}*, *[NimB4]*), *draper$^{\Delta 5}$* and *NimC1^{1}*, *eater^{1}* macrophages from L3 wandering were incubated with Alexa555 fluorescent apoptotic bodies for 30, 60, or 120 min at room temperature. Phagocytosis was quantified by flow cytometry. Data are represented as mean ± SD from three independent experiments (*$P < 0.05$, **$P < 0.01$, ****$P < 0.0001$ by ANOVA test followed by *post hoc* Dunnett's multiple comparison tests ns: not significant).

E *Ex vivo* phagocytosis assay using AlexFluor488 *Staphylococcus aureus* Bioparticles. Wild-type, *NimB4^{sk2}*, and *NimC1^{1}*, *eater^{1}* macrophages from L3 wandering were incubated with bioparticles for 30, 60, or 120 min at room temperature. Phagocytosis was quantified by flow cytometry. Data are represented as mean ± SD from three independent experiments (****$P < 0.0001$ by ANOVA test followed by *post hoc* Dunnett's multiple comparison tests. ns: not significant).

Loss of *NimB4* inhibits phagosome maturation

The accumulation of apoptotic corpses in embryonic *NimB4*^{sk2} macrophages *in vivo* indicates impaired phagocytosis in these cells, while a reduction in phagocytosis only at late time points suggests a defect in phagosome maturation. We therefore explored if the loss of NimB4 alters the phagosome maturation process. In these experiments, we included as controls *draper*$^{\Delta 5}$ *and croquemort*$^{\Delta}$ mutants previously shown to have defective phagosome maturation (Kurant *et al*, 2008; Han *et al*, 2014). The intracellular vesicles were analyzed using the fluorochrome LysoTracker Red, which fluoresces in acidic compartments. We observed that *NimB4*^{sk2}, *draper*$^{\Delta 5}$, and *croquemort*$^{\Delta}$ but not *eater*^{1} or *NimC1*^{1} macrophages contained numerous and enlarged acidic vesicles compared to wild-type macrophages (Figs 5A and B, and EV4A). To study possible NimB4 interactions with phagocytic receptors, we measured LysoTracker signal in macrophages double mutants for *NimB4*^{sk2} and *draper*$^{\Delta 5}$, *croquemort*$^{\Delta}$, *eater*^{1}, or *NimC1*^{1} (Fig EV4A). We observed an increased LysoTracker signal in the *NimB4*^{sk2}*; draper*$^{\Delta 5}$ mutant suggesting that Draper and NimB4 additively contribute to phagosome maturation. The *NimB4*^{sk}*, croquemort*$^{\Delta}$ double mutants did not show any increased LysoTracker signal compared to the single mutants. This result suggests that Croquemort and NimB4 might work together in the phagosome maturation process.

The accumulation of intracellular vesicles in *NimB4*^{sk2} macrophages was rescued by complementing the mutant with a transgene containing a wild-type copy of *NimB4* gene (Fig EV4B and C). In addition, silencing *NimB4* using RNAi with the *Hml-Gal4* macrophage driver reproduced this phenotype, confirming that the accumulation of intracellular vesicles was indeed caused by the inactivation of *NimB4* in macrophages (Fig EV4D and E). We next analyzed the subcellular morphology of *NimB4*^{sk2} intracellular vesicles by transmission electron microscopy. *NimB4*^{sk2} but not wild-type macrophages were filled with large intracellular vesicles that occupied most of the cell volume. These vesicles were surrounded by a single lipid bilayer and had a clear lumen (Fig 5C and D). A similar vesicle accumulation was also observed upon silencing of *NimB4* by RNAi (Fig EV4F and G). To confirm that this phenotype was not linked to a defect due to loss of *NimB4* during development, we used a temperature-inducible macrophages driver (*Hml*Δ^{ts}) to express *NimB4*-RNAi after the second-instar larval (L2) stage. LysoTracker staining showed that hemocytes in which *NimB4* was inactivated after the L2 stage also showed accumulation of acidic vesicles (Fig EV4H and I). Therefore, we conclude that the accumulation of acidic vesicles in *NimB4* macrophages is not caused by a defect at the early stages of development.

NimB4 plays a crucial role in phagosome–lysosomes fusion

Phagosome maturation culminates in the fusion of the phagosome with lysosomes, leading to the formation of an acidic phagolysosome. The formation of phagolysosomes is a necessary step to ensure efficient digestion of apoptotic corpses (Zhou & Yu, 2008). During phagosome maturation, the transition from early phagosome to late phagosome is marked by the conversion of Rab5 to Rab7. In addition, the phagosome acquires Lamp1, which is required for phagolysosome fusion (Huynh *et al*, 2007). Our observation that accumulated vesicles in *NimB4*^{sk2} macrophages are LysoTracker-positive and have therefore initiated acidification suggests that NimB4 is required at a later stage of phagosome maturation. To determine more precisely the step at which maturation of *NimB4*^{sk2} phagosomes is blocked, we tested whether Rab7, a marker of late phagosomes, was enriched on the vesicular membrane of *NimB4*^{sk2} macrophages. We observed that the enlarged vesicles of *NimB4*^{sk2} macrophages were positive for Rab7^{EYFP}, confirming that phagosomes are blocked at a late stage of maturation (Fig 5E and F). To determine whether fusion between the phagosome and lysosomes requires NimB4, we analyzed the fate of wild-type, *NimB4*^{sk2}, and *draper*$^{\Delta 5}$ macrophages stained with the phagosome marker LysoTracker and the lysosome marker Lamp1-mcherry. In wild-type macrophages, these markers colocalized, indicating correct formation of the phagolysosomes. In contrast, we found no colocalization of LysoTracker and Lamp1-mcherry in the *NimB4*^{sk2} and *draper*$^{\Delta 5}$ macrophages (Fig 6A and B). The Lamp1-mcherry lysosomal signals appeared as small punctate structures between the LysoTracker-positive vacuoles. This suggests that a loss of *NimB4* or *draper* impairs the fusion rather than the clustering of phagosomes with lysosomes (Fig 6A and B). An increased Lamp1-mcherry fluorescent signal in *NimB4*^{sk2} mutant macrophages indicated that the blockage of phagolysosome fusion was not due to a reduced number of lysosomes in the *NimB4*^{sk2} mutant. Interestingly, we observed a similar increase in the number of Lamp1-mcherry-positive structures when wild-type macrophages were pre-treated with chloroquine, a drug that inhibits endosomal acidification, which is used here to block phagosome maturation (Fig EV5A and B).

The fusion of the phagosome with the lysosome allows the acidification of the phagosome. We therefore assessed the acidification of phagosomes in both *NimB4*^{sk2}*, draper*$^{\Delta 5}$, and wild-type macrophages. For this, we used apoptotic cells labeled with pHrodo-succinimidyl ester (SE), a pH-sensitive fluorescent dye. We then assessed the acidification of the phagosome measuring the mean fluorescence intensity at 1 h after incubation as the *NimB4*^{sk2} mutant did not show phagocytosis defect at this time point. We observed by flow cytometry a reduced fluorescence intensity in the *NimB4*^{sk2} and the *draper*$^{\Delta 5}$ mutant compared to wild type consistent with defective acidification of the phagosome (Fig 6C).

We repeated the same experiment with pHrodo bioparticles labeled with *S. aureus* as the *NimB4*^{sk2} mutant previously showed no defect in the phagocytosis of *S. aureus* Alexa Fluor 488 BioParticles (Fig 6D). We observed by flow cytometry a reduced fluorescence intensity of pHrodo-labeled *S. aureus* bioparticles in the *NimB4*^{sk2} mutant macrophages compared to wild type (Fig 6D) consistent with defective acidification of the phagosome.

It has been shown that overexpression of Rab7 efficiently promotes the phagosome-lysosome fusion (Harrison *et al*, 2003). We therefore investigated whether increased expression of Rab7 could rescue the phagosome-lysosome fusion defect of *NimB4*^{sk2} macrophages. Overexpression of Rab7, but not Rab5, strongly reduced the number of accumulated vacuoles in *NimB4*^{sk2} macrophages, showing that promoting the phagosome-lysosome fusion is sufficient to rescue the *NimB4*^{sk2} cells (Fig 7A–C). In this experiment, we found that the overexpression of *Rab5* in wild-type macrophage has a pronounced defect on its own as previously described (Bucci *et al*, 1992). We conclude that NimB4 is required for the late stage of phagosome maturation and more specifically, for the fusion of the phagosome and lysosome.

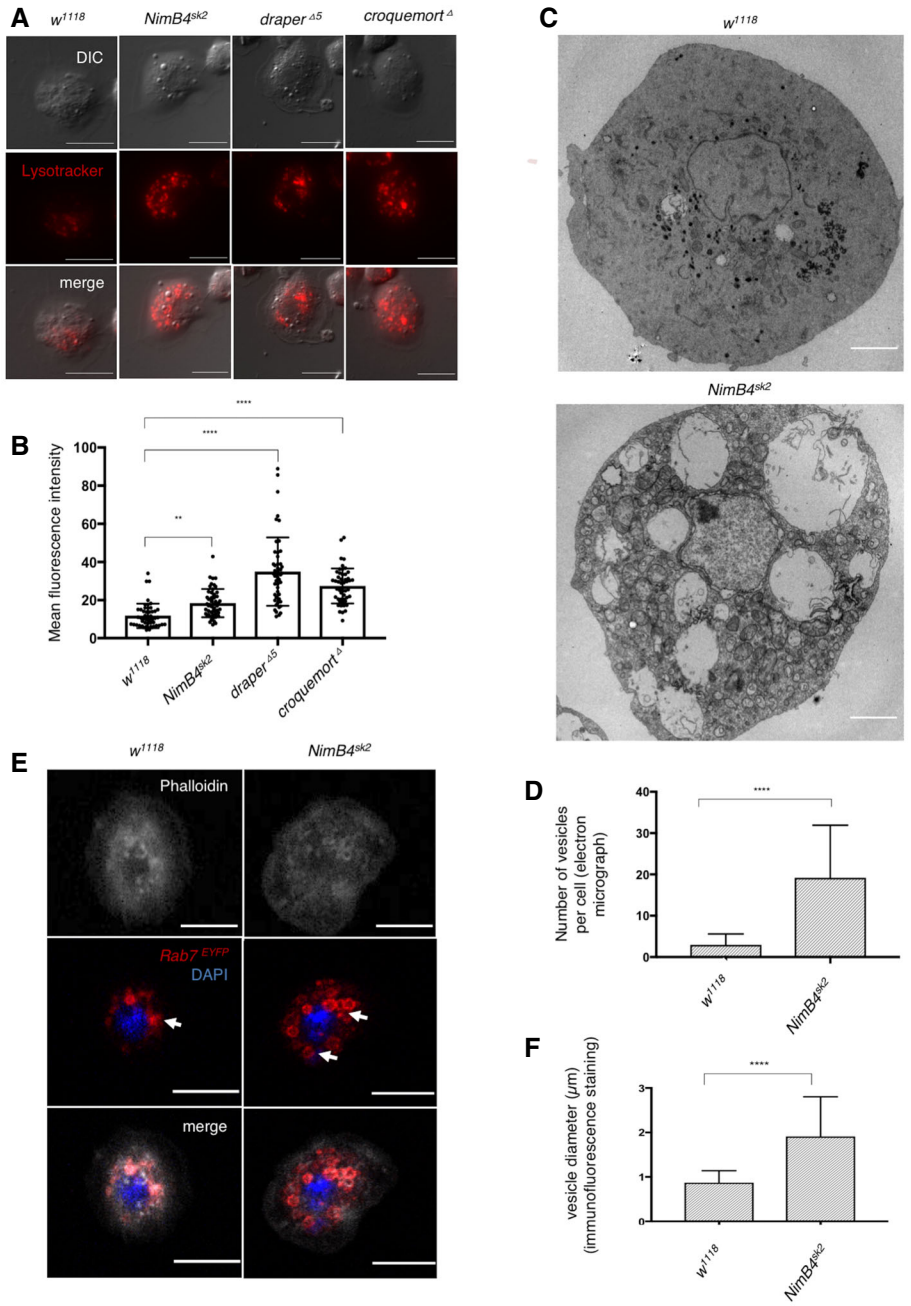

Figure 5. *NimB4^{sk2}* mutant macrophages have an increased number of vesicles.

A Representative fluorescence microscopy images of wild-type (w^{1118}), *NimB4^{sk2}*, *draper$^{\Delta 5}$*, *eater^{1}*, and *croquemort$^{\Delta}$* third-instar larvae macrophages stained with LysoTracker Red (live imaging). Overlay of fluorescence and differential interference contrast microscopy (DIC). Scale bar = 10 μm.

B Mean fluorescence intensity after staining with LysoTracker Red (live confocal imaging). Values from at least three independent experiments are represented as mean ± SD (**$P < 0.01$, ****$P < 0.0001$ by ANOVA test followed by *post hoc* Dunnett's multiple comparison tests).

C Representative transmission electron micrographs of macrophages from wild-type (top, w^{1118}) and *NimB4^{sk2}* (bottom) L3 wandering larvae. Scale bar: 2 μm.

D Quantification of the number of vesicles per macrophages in the electron micrographs. Values from at least three independent experiments are represented as mean ± SD (****$P < 0.0001$ by Mann–Whitney test).

E Representative confocal imaging of *Rab7^{EYFP}* immunostaining in *wild*-type (w^{1118}) and *NimB4^{sk2}* macrophages. Tissues were stained with anti-GFP (red, Rab7), counterstained with phalloidin (gray) and DAPI (blue). The arrows indicate the enlarged vesicles are decorated with *Rab7^{EYFP} in the NimB4^{sk2}* macrophages. Scale bar = 10 μm.

F Quantification of the diameter of the vesicles. Values from at least three independent experiments are represented as mean ± SD (****$P < 0.0001$ by Mann–Whitney test).

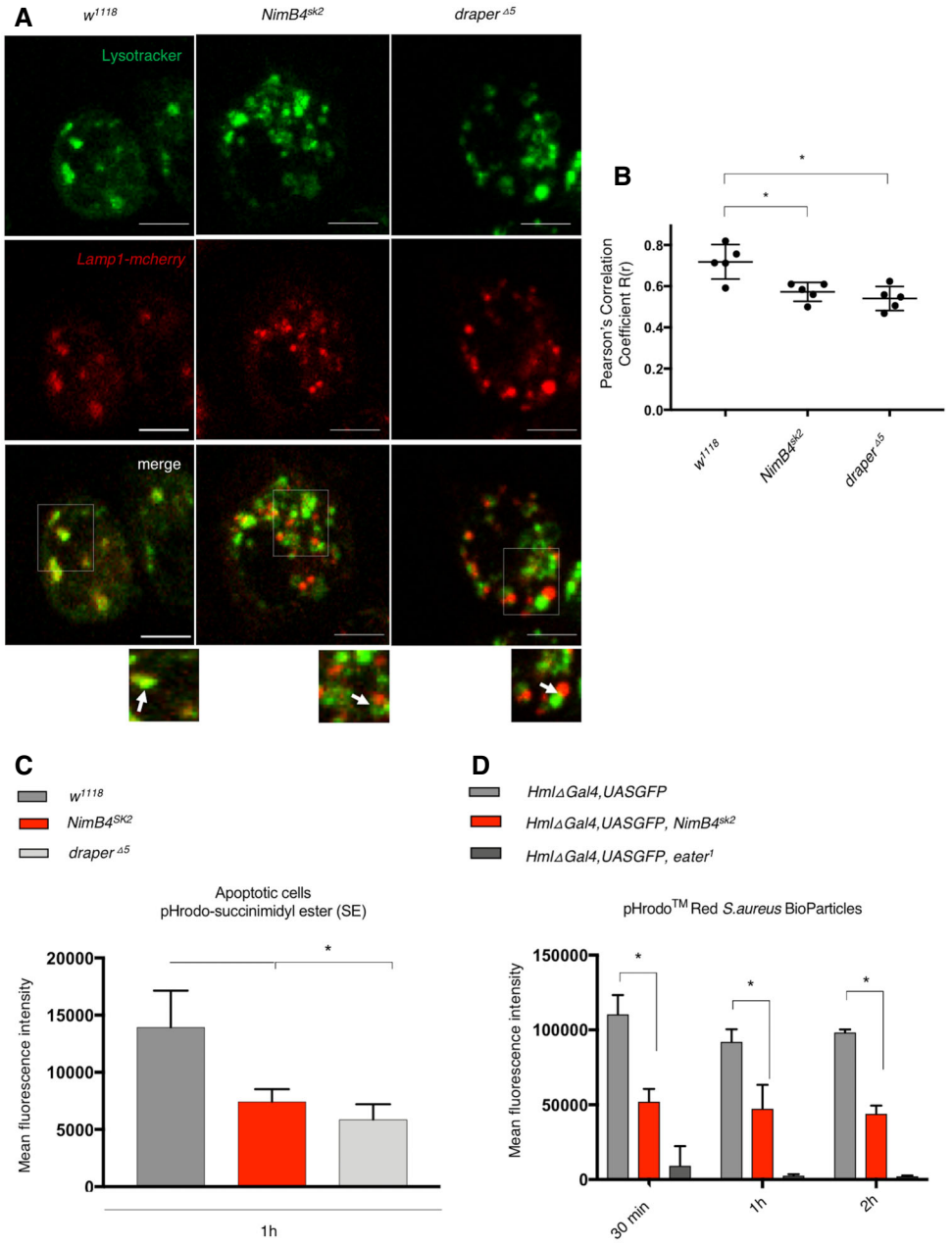

Figure 6. Loss of NimB4 blocks the phagosome maturation process by impairing the phagosome-lysosome fusion.

A Representative confocal imaging of localization of Lamp1-mcherry and LysoTracker Green in wild-type (w^{1118}), *NimB4* ^{sk2}, *and draper*$^{\Delta 5}$ macrophages (live imaging). The arrows indicate the colocalization (w^{1118}) or the clustering (*NimB4*^{sk2} *and draper*$^{\Delta 5}$) of Lamp1-mcherry and LysoTracker Green signals. Scale bar: 10 μm.

B Quantification of the colocalization of Lamp1-mcherry with LysoTracker Green, as measured by Pearson's correlation coefficient between the two signals. Values from at least five independent experiments are represented as mean ± SD (*$P < 0.05$ by ANOVA test followed by *post hoc* Dunnett's multiple comparison tests).

C *Ex vivo* phagocytosis assay using apoptotic cells labeled with pHrodo™ Red. Wild-type (w^{1118}), *NimB4*^{sk2,} and *draper*$^{\Delta 5}$ macrophages from L3 wandering larvae were incubated with pHrodo™ Red apoptotic cells for 60 min at room temperature. Phagocytosis was quantified by flow cytometry. Data are represented as mean ± SD from three independent experiments (*$P < 0.05$ by ANOVA test followed by *post hoc* Dunnett's multiple comparison tests. ns: not significant).

D *Ex vivo* phagocytosis assay using pHrodo™ Red *Staphylococcus aureus* Bioparticles™ conjugates. Wild-type, *NimB4*^{sk2} and *NimC1*^{1}, *eater*^{1} *HmlΔ-Gal4 > UAS-GFP* macrophages from L3 wandering larvae were incubated with pHrodo™ Red *S. aureus* Bioparticles™ for 30, 60, or 120 min at room temperature. Phagocytosis was quantified by flow cytometry. Data are represented as mean ± SD from three independent experiments (*$P < 0.05$ by ANOVA test followed by *post hoc* Dunnett's multiple comparison tests. ns: not significant).

Discussion

The clearance of apoptotic cells by phagocytes is a critical event during the development of all multicellular organisms. Failure in this process can lead to autoimmune or neurodegenerative diseases. In this study we identified a secreted protein of the Nimrod family, NimB4, that binds to apoptotic corpses in a PS-dependent manner to promote efferocytosis. Similar to mutants of the phagocytic receptor Draper, the *NimB4*^{sk2} mutant accumulates apoptotic cells in both embryonic and larval macrophages. Further functional studies reveal its role in phagosome maturation, notably the formation of the phagolysosome. Our study identifies the first secreted factor involved in the phagocytosis of apoptotic cells in *Drosophila,* resembling in many respects the bridging molecules found in mammals.

NimB4 is a secreted factor that promotes the phagocytosis of apoptotic cells

NimB4 was initially identified as a secreted member of the Nimrod family of unknown function. Our results show that *NimB4* is expressed in macrophages and glial cells, and that its expression is induced upon injury, a stimulus associated with increased apoptosis (Steller, 2008). In mammals, the expression of the gene encoding the bridging molecule MFG-E8 is regulated by a "find me factor" released by apoptotic cells (Miksa *et al*, 2007). Further study should identify the signaling pathway regulating *NimB4* upon injury and test whether *Drosophila* "find me factor" are involved in this process (Ravichandran, 2010, 2011).

We also observed that NimB4 is secreted by macrophages and that it is likely associated with the endosomal compartments intracellularly. *NimB4* mutants display a shorter lifespan and a locomotor defect that can be causally linked to defective apoptotic cell clearance during development and aging. These phenotypes are very similar to those previously described for *draper* mutants, albeit slightly weaker (Kurant *et al*, 2008; Draper *et al*, 2014; Etchegaray *et al*, 2016).

Our data also indicate that NimB4 binds to apoptotic corpses in a PS-dependent manner. As a member of the Nimrod family, NimB4 shares homology with SIMU and Draper, two phagocytic receptors

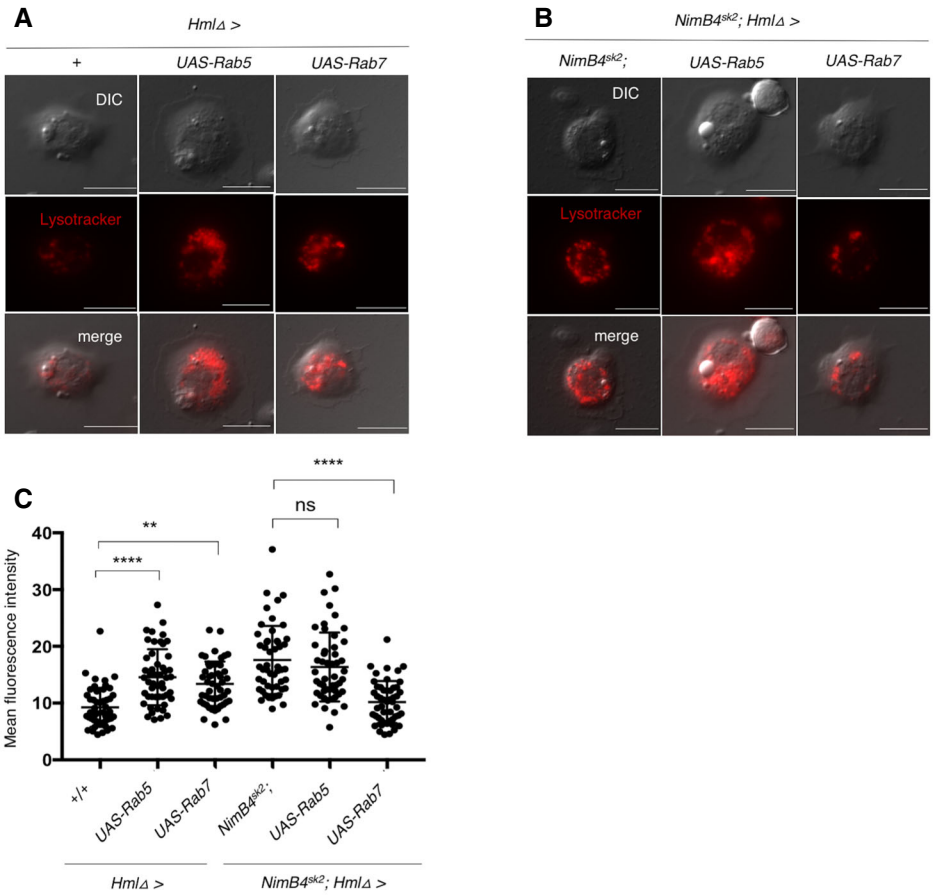

Figure 7. The increased expression of RAB7 rescues the phagosomes accumulation in *NimB4*^{sk2} macrophages.

A–B Representative fluorescence microscopy images of wild-type (A) or *NimB4*^{sk2} *(B)* macrophages expressing Rab5 (middle panel) or Rab7 (right panel) driven by *HmlΔ-Gal4 and* stained with the LysoTracker Red (live imaging). Overlay of fluorescence and DIC. Scale bar = 10 μm.

C Quantification of the mean fluorescence intensity of LysoTracker in macrophages from larvae (confocal live imaging). Values from at least three independent experiments are represented as mean ± SD (**$P < 0.01$, ****$P < 0.0001$ by ANOVA test followed by *post hoc* Dunnett's multiple comparison tests. ns: not significant).

that also interact with PS (Shklyar *et al*, 2013a; Tung *et al*, 2013). This suggests that the common EGF/Nimrod domain found in Nimrod family members may contribute to binding PS. However, it is unclear whether NimB4 binds to apoptotic cells alone and interacts directly with receptors involved in efferocytosis, or whether other co-factors are required. It is worth noting that the *Drosophila* genome encodes several other secreted NimB proteins such as NimB1, NimB2, and NimB3 that are not yet characterized (Somogyi *et al*, 2008). It is tempting to speculate that some of these proteins could work synergistically with NimB4 in the process of efferocytosis. The similarities between the $NimB4^{sk2}$ and $draper^{\Delta 5}$ mutant phenotypes suggest that both proteins function in a similar efferocytosis pathway. In this study, we did not find any evidence that NimB4 interacts with Draper. Future studies should address whether NimB4 establishes a direct bridge between apoptotic corpses and phagocytic receptors.

NimB4 is specifically required for the phagocytosis of apoptotic cells

NimB4 is required for the phagocytosis of apoptotic cells but not bacteria. This indicates that it is not a core component of the phagocytic machinery. This result is in line with many studies that show that the phagocytic process is multi-faceted and is tailored to the nature of the ingested particle. For instance, studies have shown that phagosomes containing apoptotic cells mature faster than those containing opsonized viable cells (Erwig *et al*, 2006). These observations indicate that phagocytic targets can differentially affect the maturation rate, perhaps through the recruitment of different phagocytic receptors. In contrast to NimB4, Draper contributes to the phagocytosis of both bacteria (*S. aureus*) and apoptotic cells (Manaka *et al*, 2004b; Shiratsuchi *et al*, 2012), pointing to more versatile functions. In this study, we incidentally showed that NimC1 and Eater, two immune receptors implicated in the phagocytosis of microbes, are also required for the efferocytosis process. In contrast, the role of SIMU seems to be restricted to apoptotic cell clearance during embryonic and early adult phase development (Kurant *et al*, 2008). These authors speculated that the presence of SIMU reinforces uptake of apoptotic cells at critical developmental stages characterized by massive apoptosis. We hypothesize that, like SIMU, NimB4 may have a more specific function related to a particular efferocytosis program.

The secreted NimB4 participates in phagosome maturation

Importantly, our study shows that secreted NimB4 binds to apoptotic cells and is an essential component of the machinery that promotes efferocytosis. Thus, as observed in mammals and *C. elegans*, our study reveals that secreted factors contribute to the apoptotic cell clearance in *Drosophila*. However, NimB4 is not required for macrophages binding to apoptotic bodies. Instead, apoptotic corpse uptake is reduced only at late time points. We hypothesize that this phenotype is a secondary consequence of a defect in phagosome maturation. The accumulation of immature phagosomes that are not properly eliminated would indirectly impair the uptake of new apoptotic corpses. Efferocytosis would then be impaired only at late time points when the accumulation of phagosomes reaches a threshold preventing further phagocytosis. Phagosome maturation is punctuated by two main events: the Rab5-Rab7 conversion and the fusion between the phagosome and the lysosome (Vieira *et al*, 2002; Kinchen & Ravichandran, 2008; Akbar *et al*, 2011; Pauwels *et al*, 2017; Pradhan *et al*, 2019). Interestingly, overexpression of Rab7 rescues the phagosome maturation blockage of *NimB4* mutant. Our study suggests that NimB4 is required late in the process, at the step of phagosome-lysosome fusion. Interestingly, the receptors Draper and Croquemort, initially thought to be involved in the early phase of phagocytosis, were later shown to be critical for phagosome maturation (Kurant *et al*, 2008; Han *et al*, 2014). How those receptors and NimB4 contribute to the maturation of phagosome is currently unknown. We speculate that the binding of NimB4 to apoptotic cells could orient the maturation process; that is, apoptotic corpses may require specific "digest me" signals similar to the "eat-me" signals that are required for uptake. Several mechanisms could explain how a secreted factor can impact phagosome maturation. Binding of NimB4 to apoptotic cells could cluster phagocytic receptors or activate a specific phagocytic receptor that initiates a dedicated digestion program affecting the degradation speed of ingested apoptotic cells. Alternatively, NimB4 could promote phagocytosis and lysosome maturation independently by interacting with different partners in the phagocytic process.

Is NimB4 a bridging molecule?

Bridging molecules recognize "eat-me" signals on apoptotic cells facilitating their uptake by phagocytic receptors (Ravichandran, 2010). In mammals, several soluble bridging molecules such as MFG-E8, Gas6, and protein S mediate recognition of apoptotic cells by cross-linking the PS "eat-me" signal with specific phagocytic receptors. For instance, MFG-E8 binds to the integrin receptor of phagocytic cells (Hanayama *et al*, 2002; Akakura *et al*, 2004; Nandrot *et al*, 2007). In *C. elegans,* the protein TTR-52 bridges the surface-exposed PS on apoptotic cells and the CED-1 receptor on phagocytes, which mediates recognition and engulfment of apoptotic cells (Wang *et al*, 2010). While the initial concept viewed bridging molecules as opsonins dedicated to the uptake of apoptotic cells, recent studies suggest greater complexity. Similar to NimB4, subsequent studies showed that MFG-E8 is required in the maturation phase of phagocytosis as well as in the recognition step. While apoptotic cells ingested by wild-type dendritic cells rapidly fused with lysosomes, in dendritic cells deficient for MFG-E8 smaller fragments of apoptotic cells persisted in endosomes (Peng & Elkon, 2011). NimB4 shares key features of bridging molecules, in that it is secreted by phagocytic cells, binds to apoptotic cells in the PS-dependent manner, and is specifically required for efficient efferocytosis.

Although this study has not conclusively demonstrated that NimB4 interacts with phagocytic receptors as mammalian bridging molecules do (Boada-Romero *et al*, 2020), our results reveal the importance of secreted factors that enhance efferocytosis and reinforce the notion that "bridging molecules" could play a broader role than initially thought, in orienting phagosome maturation. Future studies should characterize how secreted factors promote and direct the process of efferocytosis, and *Drosophila* offers a powerful system to address these questions.

Materials and Methods

Reagents and Tools table

Reagent/Resource	Reference or Source	Identifier or Catalog Number
Experimental models		
DrosDel w^{1118} isogenic (wild type)	Gift from Luis Teixeria (Pais, 2018)	N/A
w^{1118}; NimB4 ^{sk2}	This study	N/A
w^{iso}; NimB4^{sk2} (isogenized in the DrosDel background)	This study	N/A
w; UAS-NimB4 IR	VDRC	106392
w, UAS-NimB4	This study	N/A
w; UAS-NimB4-RFP	This study	N/A
w;; UAS-NimB4-HA	This study	N/A
w; NimB4 ^{sk2}, UAS-NimB4-RFP	This study	N/A
w; NimB4 ^{sk2}; UAS-NimB4-HA	This study	N/A
w; NimB4 ^{sk2}, [NimB4]	This study	N/A
*w;; NimB4-sGFP-V5 (*Injection in VK33 attP docking site)	This study	pFLYFOS 8882336809946705
w^{1118};; eater^{1}	Bretscher *et al* (2015)	N/A
w^{1118}; NimC1^{1}	Melcarne *et al* (2019b)	N/A
draper$^{\Delta 5}$	Gift from M. Freeman (Freeman, 2015)	N/A
; croquemort $^{\Delta}$	Gift from Yuh-Nung jang (Han *et al*, 2014)	N/A
w^{1118}; NimC1^{1}; eater^{1}	Melcarne *et al* (2019b)	N/A
w; HmlΔ-Gal4, UAS-GFP;	Sinenko and Mathey-Prevot (2004)	N/A
w;; HmlΔ-Gal4	Sinenko and Mathey-Prevot (2004)	N/A
; Tub-gal80^{ts}, UAS-GFP; HmlΔ-Gal4	This study	N/A
w; HmlΔ -Gal4, UAS-GFP, NimB4 ^{sk2}	This study	N/A
w^{1118}; NimC^{1}, HmlΔGal4,UAS-GFP;eater^{1}	Melcarne *et al* (2019b)	N/A
w; *NimB4^{sk2}; HmlΔ-Gal4*	This study	N/A
*; Tub-gal80^{ts},UAS-GFP; Lpp-Gal4/TM3 (*Referred to as *Lpp^{ts}*)	Brankatschk *et al* (2018)	N/A
;; Lpp-Gal4/TM3	N/A	N/A
; NimB4^{sk2}; Lpp-Gal4/TM3	This study	N/A
; Act5c-gal4/cyoGFP	Bretscher *et al* (2015)	N/A
*; UAS-SP$^{\mu kg}$-RFP.3.1; (*30 first amino acids of Viking protein followed by RFP)	Gift from Pastor-Parja I (Liu *et al*, 2017)	N/A
;; Df(3L)H99, kni$^{ri\text{-}1}$ p^{p}/TM3, Sb^{1}	DGGR	106395
; NimB4^{sk2} ; Df(3L)H99, kni$^{ri\text{-}1}$ p^{p}/TM3, Sb^{1}	This study	N/A
; tubGal80^{ts}; repoGal4	Hakim-Mishnaevski *et al* (2019)	N/A
w^{1118};; TI{TI}Rab7[EYFP]	BDSC	62545
w^{1118}; NimB4^{sk2}; TI{TI}Rab7[EYFP]	This study	N/A
yw; UAS-Rab5-YFP	Bloomington	9771
yw; UAS-Rab5-YFP, NimB4^{sk2}	This study	N/A
; UAS-venus-rab7	Gift from Brian McCabe	N/A
; UAS-venus-rab7, NimB4 ^{sk2}	This study	N/A
;; Lamp1–mCherry	Gift from Gábor Juhász (Lőw *et al*, 2013)	N/A
; NimB4^{sk2}; Lamp1–mCherry	This study	N/A
Iso; iso; TM2/TM6	Gift from Luis Teixeira	N/A

Reagents and Tools table (continued)

Reagent/Resource	Reference or Source	Identifier or Catalog Number
FM7; iso; iso	Gift from Luis Teixeira	N/A
Iso; Gla/cyo; iso	Gift from Luis Teixeira	N/A
Recombinant DNA		
pENTR/D-TOPO	Invitrogen	K240020
pTW	DGRC	1129
pTWR	DGRC	1136
pOT2-CG16873 Full length cDNA clone	DGRC	IP09831
pCaSpeR4	Our collection	N/A
BACR09N24	BACPAC Resources Center	RP98-9N24
Antibodies		
Chicken anti-GFP	Abcam	Cat# ab13970
Rabbit monoclonal anti-SIMU antibody	Shklyar *et al* (2013b)	N/A
Mouse monoclonal anti-Draper antibody	Kurant *et al* (2008)	N/A
Rabbit anti Dcp-1 antibody	Cell Signaling	Cat # 9578
Mouse monoclonal anti mCherry antibody	Invitrogen	Cat #M11217
Goat anti-Mouse IgG (H+L) Secondary Antibody, HRP	Jackson ImmunoResearch labs	Cat# **31430**
Goat anti-Chiken IgY (H+L) Secondary antibody, Alexa Fluor 488	Thermo Fisher Scientific	Cat# A11039
Goat anti-Mouse IgG (H+L) Highly Cross-adsorbed Secondary Antibody, Alexa Fluor 555	Thermo Fisher Scientific	Cat# A21424
Goat anti-Rabbit IgG (H+L) Highly Cross-adsorbed Secondary Antibody, Alexa Fluor 555	Thermo Fisher Scientific	Cat# A32731
Oligonucleotides and sequence-based reagents		
NimB4 F deletion screen: CGA TCT CTG TGC CTC CAC TC	Microsynth	N/A
NimB4 R deletion screen CTT GCA ACA AAC CTC GAT CA	Microsynth	N/A
NimB4 deletion screen CCC AAC GGT TTG TCC GGA ACA TC	Microsynth	N/A
NimB1 qRT F CGG CCA AAG TGT GAG AGA TT	Microsynth	N/A
NimB1 qRT R TAT CGT CAC AGC TTC CGT TC	Microsynth	N/A
NimB2 qRT F GAG TGT CTG CCG AAG TGT GA	Microsynth	N/A
NimB2 qRT R TCA CAT ATC CGG TCT TGC AG	Microsynth	N/A
NimB3 qRT F TCC CAA CTC CAG AAA TCG TC	Microsynth	N/A
NimB3 qRT R AGC AGT CCT CCG AGC AAA T	Microsynth	N/A
NimB4 qRT F TTG TGC TCA ACT ACC GCA AC	Microsynth	N/A
NimB4 qRT R CGT CCA GCT CGT ATC CCT TA	Microsynth	N/A
NimB5 qRT F CGT AAC GAC AAC GGT GAC TG	Microsynth	N/A
NimB5 qRT R GTC TCG TCC AGC TTG TAG CC	Microsynth	N/A
RpL32 qRT F GAC GCT TCA AGG GAC AGT ATC TG	Microsynth	N/A

Reagents and Tools table (continued)

Reagent/Resource	Reference or Source	Identifier or Catalog Number
RpL32 qRT R AAA CGC GGT TCT GCA TGA G	Microsynth	N/A
NimB4_gateway cloning F CAC CAT GTC AAC AAT ACT GCG A	Microsynth	N/A
NimB4_gateway cloning R CAA CCA CCA CAT ATC GCT GAG	Microsynth	N/A
Chemicals, enzyme and other reagents		
PrimeScript RT	TAKARA	Cat# RR037B
CFSE (5(6)-CFDA/SE	Thermo Fisher Scientific	Cat# C34554
CellTracker™ Red CMTPX dye	Thermo Fisher Scientific	Cat# C34572
pHrodo™ Red, succinimidyl ester	Invitrogen	Cat# P3660
Triton-X-114 (10% solution)	Thermo Scientific	Cat# 28332
Complete protease inhibitor	Sigma	11697498001
4',6-Diamidino-2-phenylindole dihydrochloride (DAPI)	Sigma	Cat# D9542
AlexaFluor 488 Phalloidin	Life Technologies	Cat# A22287
AlexaFluor 555 Phalloidin	Life Technologies	Cat# A34055
LysoTracker® Red DND-99	Thermo Fisher Scientific	Cat# L7528
LysoTracker® Green DND-26	Thermo Fisher Scientific	Cat# L7526
phenylmethylsulfonyl fluoride	Sigma	P7626
AlexFluor™ 488 *S. aureus* Bioparticles™	Thermo Fisher Scientific	Cat# s23371
pHrodo™ Red *S. aureus* Bioparticles™	Thermo Fisher Scientific	Cat# A10010
Software		
Prism 5	GraphPad Prism	N/A
Fiji 2.1.0/1.53c	Image J	N/A
Others		
Tecan Infinite M200	Tecan	N/A
Leica SP8 IN1	Leica	N/A
The Zeiss AxioImager Z1	Zeiss	N/A

Methods and Protocols

Drosophila rearing conditions

All *Drosophila* stocks were maintained at 25°C on standard fly medium consisting of 6% cornmeal, 6% yeast, 0.6% agar, 0.1% fruit juice (consisting of 50% grape juice and 50% multifruit juice), supplemented with 10.6 g/l moldex and 4.9 ml/l propionic acid. Third-instar (L3) wandering larvae were selected at 110–120 h AEL.

Mutant and transgenic lines generation

$NimB4^{sk2}$ flies were generated using the CRISPR/Cas9 technique as previously described (Kondo & Ueda, 2013). Briefly, a transgenic fly line expressing Cas9 protein using the germline-specific *nanos* promoter was crossed to a line expressing a custom guide RNA (gRNA). The cross-produces offspring with an active Cas9–gRNA complex specifically in germ cells, which cleaves and mutates the genomic target site. The following gRNA sequence was used: GGTTTGTCGCTGCCCCGGAG. To avoid any background effects, we introgressed $NimB4^{sk2}$ mutant into the w^{1118} DrosDel isogenic background for seven generations. For complementation studies, the genomic region of *NimB4* was amplified from genomic DNA including 2 kb upstream and 2 kb downstream of the *NimB4* coding sequence. Gibson assembly was used to clone the fragment into a pUAST-attB-GFP-V5-His backbone (Rauskolb *et al*, 2011). The *NimB5* and *NimB3* genes present in the upstream and downstream sequence of *NimB4*, respectively, were inactivated by directed mutagenesis. Mutagenic primers were designed to delete the G of the ATG start codon of *NimB3* and to add GA in position 44 of *NimB5* to generate non-sense coding sequences. The plasmid was then microinjected in the VK33 attP embryos. For overexpression studies, the genomic region from the 5′UTR to the stop codon of the intronless *NimB4* gene was amplified from BACR09N24 and cloned into the pDONR207 Gateway vector (Invitrogen, Carlsbad, CA, USA) and subcloned in the pTW (*Drosophila* Genomics Resource Center plasmid) transgenesis vector and used to generate transgenic *UAS-NimB4* flies. For the *UAS-NimB4-RFP*, the NimB4 cDNA sequence without STOP codon was cloned into the entry vector pENTR/D-Topo (Invitrogen) and subsequently shuttled into the RFP expression vectors pTWR (C-terminal RFP tag), obtained from the DGRC Drosophila Gateway vector collection. Plasmids were injected either at the Fly facility platform of Clermont-Ferrand (France) or by BestGene Inc. (Chino Hills, CA, USA).

RT–qPCR experiments

For quantification of mRNA, whole third-instar larvae ($n = 8$) or dissected tissues ($n = 20$–40) were isolated by TRIzol reagent and dissolved in RNase-free water. 500ng total RNA was then reverse-transcribed in 10 ml reaction volume using PrimeScript RT (TAKARA) and a mixture of oligo-dT and random hexamer primers. Quantitative PCR was performed on cDNA samples on a LightCycler 480 (Roche) in 96-well plates using the LightCycler 480 SYBR Green I master mix (Roche Diagnostics, Basel, Switzerland). Expression values were normalized to that of *RpL32*.

Western blot

Hemolymph samples were collected as follows: Forty L3 larvae were bled on a glass slide on ice; hemolymph was recovered by dissection, mixed with 10 µl of PBS supplemented with complete protease inhibitor solution (Roche) and 1mM phenylmethylsulfonyl fluoride (Sigma) and *N*-Phenylthiourea (Sigma), and then centrifuged for 10 min at 1,000 *g*, 4°C. This was followed by a second centrifugation 5 min 10,000 *g*. Protein concentration of the samples was determined by BCA assay, and 40 µg of protein extract was separated on a 4–12% acrylamide precast Novex NuPage gel (Invitrogen) under reducing conditions and transferred to membranes (Invitrogen iBlot 2). After blocking in 5% non-fat dry milk in PBS containing 0.1% for 1 h, membranes were incubated at 4°C overnight with a mouse anti-RFP antibody (Abcam) in a 1:1,000 dilution. Anti-mouse-HRP secondary antibody (Jackson ImmunoResearch) in a 1:15,000 dilution was incubated for 45 min at room temperature. Bound antibody was detected using ECL (GE Healthcare) according to the manufacturer's instructions. Membranes were imaged on a ChemiDoc XRS+ (Bio-Rad).

Apoptotic cells preparation

The S2 cells were cultured in Schneider's insect medium (Sigma-Aldrich) containing 10% FBS (Gibco™), penicillin (Sigma-Aldrich), and streptomycin (Sigma-Aldrich) at a concentration of 100 U/ml. To induce apoptosis, cycloheximide (CHX, Sigma-Aldrich) was added at a final concentration of 50 µg/ml. 24 h after the cycloheximide treatment, the cells were isolated and removed by pelleting with centrifugation at 400 *g* for 5 min at 4°C. In order to stain the apoptotic bodies, CFSE (5(6)-CFDA/SE, Molecular Probes™, or CellTracker™ Red CMTPX dye was added to the supernatant harvested from the cells at a final concentration of 5 µM and incubated 15 min at room temperature in the dark.

pHrodo staining of apoptotic cells

Apoptotic cells were labeled with the pH-sensitive stain pHrodo™ Red, succinimidyl ester (Invitrogen), which is nonfluorescent at neutral pH and emits a strong red fluorescence (532 nm) in an acidic environment (pH 4–6). After the induction of apoptosis by cycloheximide treatment, apoptotic cells were washed twice with PBS and resuspended in PBS at 10^6 cells/ml. 1 µl of 1 mg/ml pHrodo-SE (stock solution in DMSO) was added to 50 ml of cell suspension. After incubation for 30 min at RT, cells were washed twice with PBS and resuspended in PBS.

Immunohistochemistry

For immunofluorescence, L3 larvae were dissected into 150 µl PBS pH 7.4, and macrophages were allowed to adhere on a glass slide for 40 min and fixed for 10 min in PBS containing 4% paraformaldehyde. Larval tissues were dissected in PBS and fixed for at least 1 h at room temperature in 4% paraformaldehyde in PBS. For immunostaining, fixed tissues were subsequently rinsed in PBS + 0.1% Triton X-100 (PBT), permeabilized, and blocked in PBT + 2% bovine serum albumin (BSA) for 1 h and incubated with primary antibodies in PBT + 2% BSA overnight at 4°C. After 1 h washing, secondary antibodies and DAPI were applied at room temperature for 2 h. Primary antibodies used are as follows: chicken anti-GFP (Abcam, 1:1,000), rabbit anti-SIMU 1:100 (Shklyar *et al*, 2013b)), mouse anti-Draper (Developmental Studies Hybridoma Bank, 1:100), rabbit anti-Dcp-1(cell Signaling, 1:100), Mouse anti-mCherry (Invitrogen, 1:1,000). Alexa Fluor 488 and Alexa Fluor 555-conjugated secondary antibodies (Life technologies, 1:100) were used. For the chloroquine experiment, macrophages were dissected into 150 µl PBS pH 7.4. with 50 µg/ml of chloroquine and allowed to adhere on a glass slide in this solution for 40 min. Cells were then fixed with PFA 4% and immunostained as described above. Finally, cells were stained with 1/15,000 dilution of DAPI (Sigma-Aldrich) and mounted in Dako fluorescence media. Imaginal wing disks were dissected in PBS and then fixed for 15 min at room temperature in 4% PFA in PBS. Samples were rinsed twice with PBS, stained with 1/15,000 dilution of DAPI (Sigma-Aldrich), and mounted in Dako fluorescence media.

Macrophages LysoTracker red staining

Macrophages were allowed to adhere on slides for 45 min and then incubated with 1 µM LysoTracker® Red DND-99 (Invitrogen™, L7528) or LysoTracker® Green DND-26 (Invitrogen™, L7526) in PBS for 1 min at RT. The samples were washed twice in PBS and mounted for immediate observations under fluorescence or confocal microscope.

Scanning electron microscopy

Samples for SEM were prepared as follows. Six wandering third-instar larvae were bled into 50 µl of Schneider's insect medium (Sigma-Aldrich) containing 1 µM phenylthiourea (PTU; Sigma-Aldrich). The collected hemolymph was incubated on a glass coverslip for 30 min with apoptotic cells, before being fixed for 1 h with 1.25% glutaraldehyde in 0.1 M phosphate buffer, pH 7.4. Samples were then washed in cacodylate buffer (0.1 M, pH 7.4), fixed again in 0.2% osmium tetroxide in the same washing buffer, and then dehydrated in graded alcohol series. Samples underwent critical point drying and Au/Pd coating (4 nm). Scanning electron micrographs were taken with a field emission scanning electron microscope Merlin, (Zeiss, Oerzen, Embsen, Germany).

Transmission electron microscopy

Third-instar wandering larvae were bled in 50 µl of Schneider's insect medium (Sigma-Aldrich) containing 1 µM phenylthiourea (PTU; Sigma-Aldrich). The collected hemolymph was incubated on a glass coverslip for 1 h before being fixed for 2 h with 2% paraformaldehyde + 2.5% glutaraldehyde in 0.1 M phosphate buffer, pH 7.4. Samples were then washed in cacodylate buffer (0.1 M, pH 7.4), fixed again in 1% osmium tetroxide and potassium ferrocyanide 1.5% in cacodylate buffer. After several washes in distilled water, samples were stained in 1% uranyl acetate in water, washed again, and then dehydrated in graded alcohol series (50, 70, 90, 95, 100%). Embedding was performed first in 1: 1 Hard EPON

and ethanol 100%, and afterward in pure EPON, before being embedded on coated glass slides and placed at 60°C overnight. Images were acquired with a FEI Tecnai Spirit 120 kV (FEI Company, Eagle, The Netherlands).

Binding assay with apoptotic cells

L3 wandering larvae were bled into Schneider's insect medium (Sigma-Aldrich) on a previously chilled glass slide. After larva bleeding, macrophages and apoptotic cells (CellTracker™ Red CMTPX Dye) were incubated directly on the prechilled slide, in cold Schneider's medium, on ice for 60 min. After fixation in 4% paraformaldehyde PBS, Alexa Fluor488-phalloidin staining (Molecular Probes™) was performed. Finally, cells were stained with 1/15,000 dilution of DAPI (Sigma-Aldrich) Fluorescent preparations were mounted in Dako fluorescence media.

Ex vivo larval macrophage phagocytosis assay

Ex vivo phagocytosis assays of red apoptotic cells, Alexa Fluor™ 488 *S. aureus* Bioparticles™ or pHrodo™ Red *S. aureus* Bioparticles™ conjugate for Phagocytosis (Invitrogen) were performed as follows. Five L3 wandering larvae carrying the *HmlΔgal4,UAS-GFP* macrophages marker were bled into 150 µl of Schneider's insect medium (Sigma-Aldrich) containing 1 µM phenylthiourea (PTU; Sigma-Aldrich). The macrophage suspension was then transferred to 1.5 ml low binding tubes (LoBind, Eppendorf, Hamburg, Germany). The samples were incubated, respectively, with 2×10^7 Bioparticles®-Texas Red® Conjugate from *S. aureus* Wood (Invitrogen), 1×10^6 Red-labeled apoptotic cells or 10^5 pHrodo™ Red *S. aureus* Bioparticles™ for 30, 60, or 120 min to enable phagocytosis, and then placed on ice in order to stop the reaction. Phagocytosis was quantified using a flow cytometer (BD Accuri C6 flow cytometer, Becton Dickinson biosciences, Franklin Lakes, NJ, USA) in order to measure the fraction of cells phagocytosing, and their fluorescent intensity. 75 µl volume was read in ultra-low attachment 96-well flat-bottom plates (Costar no. 3474, Corning, Midland, NY, USA) at medium speed (35 µl/min). In a first step, macrophages were identified using the *HmlΔgal4UASGFP* live staining. The fluorescence intensity of single macrophages was measured in the green channel with 488nm laser and 530/30 standard filter. The Red signal of apoptotic cells, Alexa Fluor™ 488 *S. aureus* Bioparticles™ (Invitrogen), or pHrodo™ Red *S. aureus* Bioparticles™, indicative of macrophages with effective phagocytosis, was monitored with 488 nm laser and 585/40 standard filter. At least 2,000 cells per genotype and per assay were analyzed. Results are an average of three independent experiments.

The phagocytic index was calculated as follows:

$$\text{Fraction of hemocytes phagocytosing } (f) = \frac{[\text{number of hemocytes in fluorescence positive gate}]}{[\text{total number of hemocytes}]}$$

$$\text{Phagocytic index (PI)} = [\text{Mean fluorescence intensity of hemocytes in fluorescence positive gate}] \times f.$$

Image analysis and quantification

All images used for quantification were captured with a Zeiss LSM700 microscope, and all analyses were performed using ImageJ. For quantification of the fluorescence signal intensity, the fluorescent images were first converted to 8-bit images, and the total intensity value with an identical threshold was captured and measured with ImageJ. The freehand selection tool in ImageJ was used to capture and measure the area of the macrophages. Colocalization analysis was done with the ImageJ plugin "Just another Colocalization Plugin" after channel splitting and background subtraction. Rr (Pearson's correlation coefficient), Ch1:Ch2 ratios, M1 and M2 (Manders' colocalization coefficient for channel 1 and 2) were tabulated for each image.

Crawling assay

For the crawling assay, wandering third-instar larvae were used. Each larvae was taken out of the wall of the vial using a paint brush and placed onto a 10 cm Petri dish plate containing 1.5% agar. A transparent, 1.5-cm-wide plastic ring was placed on the outer rim of the agar to prevent the animal from crawling to the edge of the plate. The animal was then left on the plate for at least 1 min to acclimate to the media. Total larval movement was followed for 1 min at 25°C.

Lifespan and behavioral assays

Lifespan experiments were repeated independently at least three times using two cohorts of 20 male flies per genotype/treatment each time. Freshly emerged flies were allowed to mate for 2 days at room temperature and sorted according to sex and genotype. Experiments were performed at 25°C, and flies were flipped to fresh vials every other day using standard medium. For climbing assays, flies were gently tapped to the bottom of a tube and filmed with a digital camera. The percentage of flies climbing above 7 cm within 10 s was calculated.

Statistical tests

Each experiment was repeated independently a minimum of three times (unless otherwise indicated), error bars represent the standard error of the mean of replicate experiments. Data were analyzed using appropriate statistical tests as indicated in figure legends using the GraphPad Prism software. Significance tests were performed using the Mann–Whitney test. For experiments with more than two conditions, significance was tested using ANOVA test followed by *post hoc* Dunnett's multiple comparison tests. *P* values of $< 0.05 = *$, $< 0.01 = **$, and $< 0.001 = ***$.

Data availability

No data were deposited in public databases.

Expanded View for this article is available online.

Acknowledgements

We thank the VDRC in Vienna, the Bloomington Stock Center (NIH P40OD018537), Brian McCabe, and Gabor Juhas for the fly stocks. We thank the BIOP platform (EPFL) and the BioEM platform (EPFL) for help with electron microscopy experiments. This work was supported by the Sinergia grant CRSII5_186397. We thank Jean-Philippe Boquete for his precious technical support, we thank Hannah Westlake for critical reading of the manuscript, and Dominique Soldati (University of Geneva) and Brian McCabe (EPFL) for stimulating discussion.

Author contributions

BP, SR, and BL conceived and designed the experiments and wrote the paper. BP, SR, KH, FM, ER, RH, MP, SK performed the experiments. BP, SR, BL, EK analyzed the data.

Conflict of interest

The authors declare that they have no conflict of interest.

References

Akakura S, Singh S, Spataro M, Akakura R, Kim J-I, Albert ML, Birge RB (2004) The opsonin MFG-E8 is a ligand for the αvβ5 integrin and triggers DOCK180-dependent Rac1 activation for the phagocytosis of apoptotic cells. *Exp Cell Res* 292: 403–416

Akbar MA, Tracy C, Kahr WHA, Krämer H (2011) The full-of-bacteria gene is required for phagosome maturation during immune defense in *Drosophila*. *J Cell Biol* 192: 383–390

Alvarez-Dominguez C, Barbieri AM, Berón W, Wandinger-Ness A, Stahl PD (1996) Phagocytosed live listeria monocytogenes influences Rab5-regulated *in vitro* phagosome-endosome fusion. *J Biol Chem* 271: 13834–13843

Arandjelovic S, Ravichandran KS (2015) Phagocytosis of apoptotic cells in homeostasis. *Nat Immunol* 16: 907–917

Boada-Romero E, Martinez J, Heckmann BL, Green DR (2020) The clearance of dead cells by efferocytosis. *Nat Rev Mol Cell Biol* 21: 398–414

Borisenko GG, Iverson SL, Ahlberg S, Kagan VE, Fadeel B (2004) Milk fat globule epidermal growth factor 8 (MFG-E8) binds to oxidized phosphatidylserine: implications for macrophage clearance of apoptotic cells. *Cell Death Differ* 11: 943–945

Bork P, Downing AK, Kieffer B, Campbell ID (1996) Structure and distribution of modules in extracellular proteins. *Q Rev Biophys* 29: 119–167

Botelho R, Fountain A, Lancaster C, Terebiznik M (2020) Clathrin-mediated phagosome resolution regenerates lysosomes and maintains degradative capacity of macrophages after phagocytosis. *FASEB J* 34: 1

Brankatschk M, Gutmann T, Knittelfelder O, Palladini A, Prince E, Grzybek M, Brankatschk B, Shevchenko A, Coskun Ü, Eaton S (2018) A temperature-dependent switch in feeding preference improves *Drosophila* development and survival in the cold. *Dev Cell* 46: 781–793.e4

Bretscher AJ, Honti V, Binggeli O, Burri O, Poidevin M, Kurucz É, Zsámboki J, Andó I, Lemaitre B (2015) The Nimrod transmembrane receptor Eater is required for hemocyte attachment to the sessile compartment in *Drosophila melanogaster*. *Biol Open* 4: 355–363

Bucci C, Parton RG, Mather IH, Stunnenberg H, Simons K, Hoflack B, Zerial M (1992) The small GTPase rab5 functions as a regulatory factor in the early endocytic pathway. *Cell* 70: 715–728

Callebaut I, Mignotte V, Souchet M, Mornon JP (2003) EMI domains are widespread and reveal the probable orthologs of the *Caenorhabditis elegans* CED-1 protein. *Biochem Biophys Res Commun* 300: 619–623

Chen P, Nordstrom W, Gish B, Abrams JM (1996) grim, a novel cell death gene in *Drosophila*. *Genes Dev* 10: 1773–1782

Davidson AJ, Wood W (2020) Phagocyte responses to cell death in flies. *Cold Spring Harb Perspect Biol* 12. a036350

Davie K, Janssens J, Koldere D, De Waegeneer M, Pech U, Kreft Ł, Aibar S, Makhzami S, Christiaens V, Bravo González-Blas C *et al* (2018) A single-cell transcriptome atlas of the aging *Drosophila* brain. *Cell* 174: 982–998.e20

Draper I, Mahoney LJ, Mitsuhashi S, Pacak CA, Salomon RN, Kang PB (2014) Silencing of drpr leads to muscle and brain degeneration in adult *Drosophila*. *Am J Pathol* 184: 2653–2661

Duclos S, Diez R, Garin J, Papadopoulou B, Descoteaux A, Stenmark H, Desjardins M (2000) Rab5 regulates the kiss and run fusion between phagosomes and endosomes and the acquisition of phagosome leishmanicidal properties in RAW 264.7 macrophages. *J Cell Sci* 113(Pt 19): 3531–3541

Elliott MR, Ravichandran KS (2010) Clearance of apoptotic cells: implications in health and disease. *J Cell Biol* 189: 1059–1070

Elliott MR, Ravichandran KS (2016) The dynamics of apoptotic cell clearance. *Dev Cell* 38: 147–160

van Engeland M, Nieland LJW, Ramaekers FCS, Schutte B, Reutelingsperger CPM (1998) Annexin V-Affinity assay: a review on an apoptosis detection system based on phosphatidylserine exposure. *Cytometry* 31: 1–9

Erwig L-P, McPhilips KA, Wynes MW, Ivetic A, Ridley AJ, Henson PM (2006) Differential regulation of phagosome maturation in macrophages and dendritic cells mediated by Rho GTPases and ezrin–radixin–moesin (ERM) proteins. *Proc Natl Acad Sci USA* 103: 12825–12830

Etchegaray JI, Elguero EJ, Tran JA, Sinatra V, Feany MB, McCall K (2016) Defective phagocytic corpse processing results in neurodegeneration and can be rescued by TORC1 activation. *J Neurosci* 36: 3170–3183

Freeman MR (2015) *Drosophila* central nervous system glia. *Cold Spring Harb Perspect Biol* 7: a020552

Freeman MR, Delrow J, Kim J, Johnson E, Doe CQ (2003) Unwrapping glial biology: GCM target genes regulating glial development, diversification, and function. *Neuron* 38: 567–580

Fuentes-Medel Y, Logan MA, Ashley J, Ataman B, Budnik V, Freeman MR (2009) Glia and muscle sculpt neuromuscular arbors by engulfing destabilized synaptic boutons and shed presynaptic debris. *PLoS Biol* 7: e1000184

Galvan MD, Greenlee-Wacker MC, Bohlson SS (2012) C1q and phagocytosis: the perfect complement to a good meal. *J Leukoc Biol* 92: 489–497

Hakim-Mishnaevski K, Flint-Brodsly N, Shklyar B, Levy-Adam F, Kurant E (2019) Glial phagocytic receptors promote neuronal loss in adult *Drosophila* brain. *Cell Rep* 29: 1438–1448.e3

Han C, Song Y, Xiao H, Wang D, Franc NC, Jan LY, Jan Y-N (2014) Epidermal cells are the primary phagocytes in the fragmentation and clearance of degenerating dendrites in *Drosophila*. *Neuron* 81: 544–560

Hanayama R, Tanaka M, Miwa K, Shinohara A, Iwamatsu A, Nagata S (2002) Identification of a factor that links apoptotic cells to phagocytes. *Nature* 417: 182–187

Harrison RE, Bucci C, Vieira OV, Schroer TA, Grinstein S (2003) Phagosomes fuse with late endosomes and/or lysosomes by extension of membrane protrusions along microtubules: role of Rab7 and RILP. *Mol Cell Biol* 23: 6494–6506

Henson PM, Hume DA (2006) Apoptotic cell removal in development and tissue homeostasis. *Trends Immunol* 27: 244–250

Hilu-Dadia R, Kurant E (2020) Glial phagocytosis in developing and mature *Drosophila* CNS: tight regulation for a healthy brain. *Curr Opin Immunol* 62: 62–68

Huang W, Wu J, Yang H, Xiong Y, Jiang R, Cui T, Ye D (2017) Milk fat globule-EGF factor 8 suppresses the aberrant immune response of systemic lupus erythematosus-derived neutrophils and associated tissue damage. *Cell Death Differ* 24: 263–275

Huynh KK, Eskelinen E-L, Scott CC, Malevanets A, Saftig P, Grinstein S (2007) LAMP proteins are required for fusion of lysosomes with phagosomes. *EMBO J* 26: 313–324

Ivy JR, Drechsler M, Catterson JH, Bodmer R, Ocorr K, Paululat A, Hartley PS (2015) Klf15 is critical for the development and differentiation of *Drosophila* nephrocytes. *PLoS One* 10: e0134620

Janko C, Jeremic I, Biermann M, Chaurio R, Schorn C, Muñoz LE, Herrmann M (2013) Cooperative binding of Annexin A5 to phosphatidylserine on apoptotic cell membranes. *Phys Biol* 10: 065006

Ju JS, Cho MH, Brade L, Kim JH, Park JW, Ha N-C, Söderhäll I, Söderhäll K, Brade H, Lee BL (2006) A novel 40-kDa protein containing six repeats of an epidermal growth factor-like domain functions as a pattern recognition protein for lipopolysaccharide. *J Immunol* 177: 1838–1845

Kinchen JM, Doukoumetzidis K, Almendinger J, Stergiou L, Tosello-Trampont A, Sifri CD, Hengartner MO, Ravichandran KS (2008) A novel pathway for phagosome maturation during engulfment of apoptotic cells. *Nat Cell Biol* 10: 556–566

Kinchen JM, Ravichandran KS (2008) Phagosome maturation: going through the acid test. *Nat Rev Mol Cell Biol* 9: 781–795

Kinchen JM, Ravichandran KS (2010) Identification of two evolutionarily conserved genes regulating processing of engulfed apoptotic cells. *Nature* 464: 778–782

Kondo S, Ueda R (2013) Highly improved gene targeting by germline-specific Cas9 expression in *Drosophila*. *Genetics* 195: 715–721

Kurucz É, Márkus R, Zsámboki J, Folkl-Medzihradszky K, Darula Z, Vilmos P, Udvardy A, Krausz I, Lukacsovich T, Gateff E *et al* (2007) Nimrod, a putative phagocytosis receptor with EGF repeats in *Drosophila* plasmatocytes. *Curr Biol* 17: 649–654

Kurant E, Axelrod S, Leaman D, Gaul U (2008) Six-microns-under acts upstream of draper in the glial phagocytosis of apoptotic neurons. *Cell* 133: 498–509

Kurant E (2011) Keeping the CNS clear: glial phagocytic functions in *Drosophila*. *Glia* 59: 1304–1311

Kusunoki R, Ishihara S, Aziz M, Oka A, Tada Y, Kinoshita Y (2012) Roles of milk fat globule-epidermal growth factor 8 in intestinal inflammation. *Digestion* 85: 103–107

Lancaster C, Fountain A, Somerville E, Sheth J, Dayam RM, Jacobelli V, Somerville A, Terebiznik M, Botelho RJ (2020) Phagosome resolution regenerates lysosomes and maintains the degradative capacity in phagocytes. *bioRxiv* https://doi.org/10.1101/2020.05.14.094722 [PREPRINT]

Levin R, Grinstein S, Canton J (2016) The life cycle of phagosomes: formation, maturation, and resolution. *Immunol Rev* 273: 156–179

Liu M, Feng Z, Ke H, Liu Y, Sun T, Dai J, Cui W, Pastor-Pareja JC (2017) Tango1 spatially organizes ER exit sites to control ER export. *J Cell Biol* 216: 1035–1049

Lőw P, Varga A, Pircs K, Nagy P, Szatmari Z, Sass M, Juhasz G (2013) Impaired proteasomal degradation enhances autophagy via hypoxia signaling in *Drosophila*. *BMC Cell Biol* 14: 29

Manaka J, Kuraishi T, Shiratsuchi A, Nakai Y, Higashida H, Henson P, Nakanishi Y (2004a) Draper-mediated and phosphatidylserine-independent phagocytosis of apoptotic cells by Drosophila hemocytes/macrophages. *J Biol Chem* 279: 48466–48476

Manaka J, Kuraishi T, Shiratsuchi A, Nakai Y, Higashida H, Henson P, Nakanishi Y (2004b) Draper-mediated and phosphatidylserine-independent phagocytosis of apoptotic cells by *Drosophila* hemocytes/macrophages. *J Biol Chem* 279: 48466–48476

Melcarne C, Lemaitre B, Kurant E (2019a) Phagocytosis in *Drosophila*: from molecules and cellular machinery to physiology. *Insect Biochem Mol Biol* 109: 1–12

Melcarne C, Ramond E, Dudzic J, Bretscher AJ, Kurucz É, Andó I, Lemaitre B (2019b) Two Nimrod receptors, NimC1 and Eater, synergistically contribute to bacterial phagocytosis in *Drosophila melanogaster*. *FEBS J* 286: 2670–2691

Miksa M, Amin D, Wu R, Dong W, Ravikumar TS, Wang P (2007) Fractalkine-induced MFG-E8 leads to enhanced apoptotic cell clearance by macrophages. *Mol Med* 13: 553–560

Nagaosa K, Okada R, Nonaka S, Takeuchi K, Fujita Y, Miyasaka T, Manaka J, Ando I, Nakanishi Y (2011) Integrin βν-mediated phagocytosis of apoptotic cells in *Drosophila* embryos. *J Biol Chem* 286: 25770–25777

Nagata S, Hanayama R, Kawane K (2010) Autoimmunity and the clearance of dead cells. *Cell* 140: 619–630

Nagata S, Suzuki J, Segawa K, Fujii T (2016) Exposure of phosphatidylserine on the cell surface. *Cell Death Differ* 23: 952–961

Nandrot EF, Anand M, Almeida D, Atabai K, Sheppard D, Finnemann SC (2007) Essential role for MFG-E8 as ligand for alphavbeta5 integrin in diurnal retinal phagocytosis. *Proc Natl Acad Sci USA* 104: 12005–12010

Nonaka S, Nagaosa K, Mori T, Shiratsuchi A, Nakanishi Y (2013) Integrin αPS3/βν-mediated phagocytosis of apoptotic cells and bacteria in *Drosophila*. *J Biol Chem* 288: 10374–10380

Pauwels A-M, Trost M, Beyaert R, Hoffmann E (2017) Patterns, receptors, and signals: regulation of phagosome maturation. *Trends Immunol* 38: 407–422

Pearson AM, Baksa K, Rämet M, Protas M, McKee M, Brown D, Ezekowitz RAB (2003) Identification of cytoskeletal regulatory proteins required for efficient phagocytosis in *Drosophila*. *Microbes Infect* 5: 815–824

Peng Y, Elkon KB (2011) Autoimmunity in MFG-E8–deficient mice is associated with altered trafficking and enhanced cross-presentation of apoptotic cell antigens. *J Clin Invest* 121: 2221–2241

Poon IKH, Lucas CD, Rossi AG, Ravichandran KS (2014) Apoptotic cell clearance: basic biology and therapeutic potential. *Nat Rev Immunol* 14: 166–180

Poteryaev D, Datta S, Ackema K, Zerial M, Spang A (2010) Identification of the switch in early-to-late endosome transition. *Cell* 141: 497–508

Pradhan G, Raj Abraham P, Shrivastava R, Mukhopadhyay S (2019) Calcium signaling commands phagosome maturation process. *Int Rev Immunol* 38: 57–69

Purice MD, Speese SD, Logan MA (2016) Delayed glial clearance of degenerating axons in aged *Drosophila* is due to reduced PI3K/Draper activity. *Nat Commun* 7: 12871

Ramond E, Petrignani B, Dudzic JP, Boquete J-P, Poidevin M, Kondo S, Lemaitre B (2020) The adipokine NimrodB5 regulates peripheral hematopoiesis in *Drosophila*. *FEBS J* 287: 3399–3426

Rauskolb C, Pan G, Reddy BVVG, Oh H, Irvine KD (2011) Zyxin links fat signaling to the hippo pathway. *PLoS Biol* 9: e1000624

Ravichandran KS (2003) "Recruitment signals" from apoptotic cells: invitation to a quiet meal. *Cell* 113: 817–820

Ravichandran KS (2010) Find-me and eat-me signals in apoptotic cell clearance: progress and conundrums. *J Exp Med* 207: 1807–1817

Ravichandran KS (2011) Beginnings of a good apoptotic meal: the find-me and eat-me signaling pathways. *Immunity* 35: 445–455

Roddie HG, Armitage EL, Coates JA, Johnston SA, Evans IR (2019) Simu-dependent clearance of dying cells regulates macrophage function and inflammation resolution. *PLoS Biol* 17: e2006741

Sarov M, Barz C, Jambor H, Hein MY, Schmied C, Suchold D, Stender B, Janosch S, Kj VV, Krishnan Rt *et al* (2016) A genome-wide resource for the analysis of protein localisation in *Drosophila*. *eLife* 5: e12068

Savill J, Fadok V (2000) Corpse clearance defines the meaning of cell death. *Nature* 407: 784–788

Segawa K, Nagata S (2015) An apoptotic 'eat me' signal: phosphatidylserine exposure. *Trends Cell Biol* 25: 639–650

Serizier SB, McCall K (2017) Scrambled eggs: apoptotic cell clearance by non-professional phagocytes in the *Drosophila* ovary. *Front Immunol* 8: 1642

Shiratsuchi A, Mori T, Sakurai K, Nagaosa K, Sekimizu K, Lee BL, Nakanishi Y (2012) Independent recognition of *Staphylococcus aureus* by two receptors for phagocytosis in *Drosophila*. *J Biol Chem* 287: 21663–21672

Shklyar B, Levy-Adam F, Mishnaevski K, Kurant E (2013a) Caspase activity is required for engulfment of apoptotic cells. *Mol Cell Biol* 33: 3191–3201

Shklyar B, Shklover J, Kurant E (2013b) Live imaging of apoptotic cell clearance during drosophila embryogenesis. *J Vis Exp* e50151

Shklyar B, Sellman Y, Shklover J, Mishnaevski K, Levy-Adam F, Kurant E (2014) Developmental regulation of glial cell phagocytic function during *Drosophila* embryogenesis. *Dev Biol* 393: 255–269

Somogyi K, Sipos B, Penzes Z, Kurucz E, Zsamboki J, Hultmark D, Ando I (2008) Evolution of genes and repeats in the nimrod superfamily. *Mol Biol Evol* 25: 2337–2347

Steller H (2008) Regulation of apoptosis in *Drosophila*. *Cell Death Differ* 15: 1132–1138

Stuart LM, Ezekowitz RAB (2005) Phagocytosis: elegant complexity. *Immunity* 22: 539–550

Troha K, Nagy P, Pivovar A, Lazzaro BP, Hartley PS, Buchon N (2019) Nephrocytes remove microbiota-derived peptidoglycan from systemic circulation to maintain immune homeostasis. *Immunity* 51: 625–637.e3

Tung TT, Nagaosa K, Fujita Y, Kita A, Mori H, Okada R, Nonaka S, Nakanishi Y (2013) Phosphatidylserine recognition and induction of apoptotic cell clearance by *Drosophila* engulfment receptor Draper. *J Biochem* 153: 483–491

Vieira OV, Botelho RJ, Grinstein S (2002) Phagosome maturation: aging gracefully. *Biochem J* 366: 689–704

Wang X, Li W, Zhao D, Liu B, Shi Y, Chen B, Yang H, Guo P, Geng X, Shang Z *et al* (2010) *Caenorhabditis elegans* transthyretin-like protein TTR-52 mediates recognition of apoptotic cells by the CED-1 phagocyte receptor. *Nat Cell Biol* 12: 655–664

Wu Y, Tibrewal N, Birge RB (2006) Phosphatidylserine recognition by phagocytes: a view to a kill. *Trends Cell Biol* 16: 189–197

Yousefian J, Troost T, Grawe F, Sasamura T, Fortini M, Klein T (2013) Dmon1 controls recruitment of Rab7 to maturing endosomes in *Drosophila*. *J Cell Sci* 126: 1583–1594

Zheng Q, Ma A, Yuan L, Gao N, Feng Q, Franc NC, Xiao H (2017) Apoptotic cell clearance in *Drosophila melanogaster*. *Front Immunol* 8: 1881

Zhou Z, Yu X (2008) Phagosome maturation during the removal of apoptotic cells: receptors lead the way. *Trends Cell Biol* 18: 474–485